DOE/NASA/2817-3
NASA CR-167925
DOT/TSC/NASA-82-3

FUEL ECONOMY AND EXHAUST EMISSIONS CHARACTERISTICS OF DIESEL VEHICLES: TEST RESULTS OF A PROTOTYPE CHRYSLER VOLARE, 225 CID (3.7-LITER) AUTOMOBILE

R,A, WALTER
U.S. DEPARTMENT OF TRANSPORTATION
RESEARCH AND SPECIAL PROGRAMS ADMINISTRATION
Transportation Systems Center
Cambridge MA 02142

JULY 1982

Prepared for
NATIONAL AERONAUTICS AND SPACE ADMINISTRATION
Lewis Research Center
Cleveland OH 44135
Under Interagency Order C-32817-D

for
U.S. DEPARTMENT OF ENERGY
Conservation and Solar Energy
Office of Vehicle and Engine R&D
Washington DC 20585

DOE/NASA/2817-3
NASA CR-167926
DOT/TSC/NASA-82-3

FUEL ECONOMY AND EXHAUST EMISSIONS CHARACTERISTICS OF DIESEL VEHICLES: TEST RESULTS OF A PROTOTYPE CHRYSLER VOLARE, 225 CID (3.7-LITER) AUTOMOBILE

R,A, WALTER
U.S. DEPARTMENT OF TRANSPORTATION
RESEARCH AND SPECIAL PROGRAMS ADMINISTRATION
Transportation Systems Center
Cambridge MA 02142

JULY 1982

Prepared for
NATIONAL AERONAUTICS AND SPACE ADMINISTRATION
Lewis Research Center
Cleveland OH 44135
Under Interagency Order C-32817-D

for
U.S. DEPARTMENT OF ENERGY
Conservation and Solar Energy
Office of Vehicle and Engine R&D
Washington DC 20585
Under Interagency Agreement DE-A101-80CS50194

Technical Report Documentation Page

1. Report No.	2. Government Accession No.	3. Recipient's Catalog No.
NASA CR 167925		

4. Title and Subtitle	5. Report Date
FUEL ECONOMY AND EXHAUST EMISSIONS CHARACTERISTICS OF DIESEL VEHICLES: TEST RESULTS OF A PROTOTYPE CHRYSLER VOLARE, 225 CID (3.7-LITER) AUTOMOBILE	JULY 1982
	6. Performing Organization Code
7. Author(s) R. A. Walter	8. Performing Organization Report No. DOT/TSC/NASA-82-3
9. Performing Organization Name and Address U.S. Department of Transportation Research and Special Programs Administration Transportation Systems Center Cambridge MA 02142	10. Work Unit No. (TRAIS)
	11. Contract or Grant No. C-32817-D
12. Sponsoring Agency Name and Address U.S. Department of Energy Conservation and Solar Energy Office of Vehicle and Engine R&D Washington DC 20585	13. Type of Report and Period Covered January 1981-June 1981 Final Report
	14. Sponsoring Agency Code DOE/NASA/2817-3

15. Supplementary Notes
Technical Report. Prepared under Interagency Agreement DE-A101-80CS50194. Project Manager R. Dezelick, Engine Systems Division, NASA Lewis Research Center, Cleveland, OH 44135

16. Abstract

This report documents the results obtained from fuel economy and emission tests conducted on a prototype Chysler Volare diesel vehicle. The vehicle was tested on a chassis dynamometer over selected drive cycles and steady-state conditions. The fuel used, was a DOE/BETC "referee" fuel. Particulate emission rates were calculated from dilution tunnel measurements and large volume particulate samples were collected for biological and chemical analysis. The vehicle obtained 32.7 mpg for the FTP urban cycle and 48.8 mpg for the highway cycle. The emissions rates were 0.42/1.58/1.17/0.28 g/mile of HC, CO, NO_x and particulates respectively.

17. Key Words	18. Distribution Statement
Diesel, Fuel Economy, Emissions, Particulates, Chassis Dynamometer, Oxidation Catalyst, Turbocharged Diesel	Unclassified-Unlimited STAR Category 85 DOE Category UC-96

19. Security Classif. (of this report)	20. Security Classif. (of this page)	21. No. of Pages	22. Price
Unclassified	Unclassified	48	

TABLE OF CONTENTS

LIST OF ILLUSTRATIONS

LIST OF TABLES

METRIC CONVERSION FACTORS

ACKNOWLEDGEMENTS

This work was sponsored by the U.S. Department of Energy and managed by the NASA Lewis Research Center under Interagency Order C-32817-D. The author wishes to acknowledge the project support work of Mr. Robert Dezelick, Project Manager, NASA Lewis Research Center, and Mr. Maurice W. Dumais and Ms. Sharon Quayle of the Automotive Research Laboratory, Transportation Systems Center.

1. INTRODUCTION

Under Interagency Order C-32817-D, the Department of Transportation, Transportation Systems Center (DOT/TSC) participated in a cooperative research program with the Department of Energy and NASA-Lewis Research Center. The objectives of this project were two-fold:

1. To determine the ability of various diesel technologies, to improve fuel efficiency, reduce exhaust emissions, and
2. To collect adequate particulate samples for chemical and biological characterization as part of the DOE Diesel Health Effects Research Program.

The vehicle used for the portion of the program discussed in this paper was a Chrysler Volare 225 CID prototype diesel. This vehicle was loaned to TSC by Chrysler through contract DOT-TSC-1423. The Chrysler diesel (rated 95 hp at 3600 rpm) was tested at the DOT/TSC Automotive Research Laboratory in a 3500-lb inertia weight configuration (Figure 1) following a matrix employed to test the Fiat 131 naturally aspirated and turbo-charged vehicles.[1&2] The car was equipped with 225 CID indirect injection diesel engine and a four-speed manual transmission. The vehicle was tested over selected drive cycles and steady-state conditions on a large-roll, chassis dynamometer. Test cycles consisted of the EPA/Federal Test Procedure Urban Cycle (FTP), the Highway Fuel Economy Test (HFET), and the New York City Cycle (NYCC). Steady-state measurements were collected at nine different speed-gear combinations. Approximately 5 grams of particulate matter were collected for use in the DOE Diesel Health Effects Research Program. (See Table A-1 in Appendix.)

FIGURE 1. CHRYSLER VOLARE DIESEL IN A 3500 LB INERTIA VEHICLE

2. EXPERIMENTAL DESIGN

2.1 TEST VEHICLE

This section describes the salient features of the Chrysler Volare Diesel (# 18M 279). For a more detailed description of the prototype vehicle and the test procedure refer to the Chrysler manufacturer's report and to Fuel Economy and Exhaust Emissions Characteristics of Diesel Vehicles; Test Results of a Prototype Fiat 131 NA 2.4-Liter Automobile.[1]

2.1.1 Engine and Vehicle Specifications

The engine, 225 CID (3.7 Liter) prototype indirect injection diesel rated at 95 hp at 3600 rpm, is a diesel conversion from the spark ignition Chrysler "slant-six" engine. The engine main specifications are given in Table 1.

The vehicle's inertia weight was 3500 pounds. Tire size was ER78-14. The Chrysler vehicle was equipped with a four speed manual transmission with gear ratios of 3.09, 1.79, 1.00, and 0.73, the axle ratio is 2.76:1. (Table 2.)

2.1.2 Manufacturer's Data on Emissions and Fuel Economy

The emissions rates measured by Chrysler at 7° BTDC static injection timing were 0.27 grams per mile of HC and 1.4 grams per mile of NO_x using the 1974 Hot FTP cycle. The manufacturer-determined fuel economy over this cycle was approximately 36 mpg. See Figures 7-9. The fuel economy results for the highway test and various steady-state conditions are given in Figure 2.

2.1.3 Fuel

The fuel used for these tests was produced by Phillips Petroleum according to the specifications of Bartlesville Energy Technology Center (BETC) for a "common lot" diesel fuel

TABLE 1. 225 IN^3 INLINE 6 CYLINDER DIESEL ENGINE ENGINE SPECIFICATIONS

Displacement, cubic inches	225
Maximum brake horsepower, bhp @ 3600	95
Maximum torque, lb-ft @ 2000	165
Bore and stroke, inches	3.401 x 4.125
Configuration	6 cyl - inline
Compression ratio	21.5:1
Firing order	1-5-3-6-2-4
Intake manifold material	Tubular - fabricated
Block material	Cast iron
Head material	Cast iron
Exhaust manifold material	Nodular cast iron
Number of crankshaft main bearings	4
Number of compression rings/piston	2
Number of oil rings/piston	1
Cam drive	Chain
Valve size:	
Intake, inches	1.58
Exhaust, inches	1.31
Valve timing:	
Intake opens, °BTC	2
Intake closes, °ABC	34
Exhaust opens, °BBC	52
Exhaust closes, °ATC	4
Valve lift (zero lash):	
Intake, inches	0.366
Exhaust, inches	0.386
Engine weight, lbs	450
Lubrication system	Rotary pump - full pressure
Crankcase emission control:	
Control method	Positive crankcase ventilation
Point of discharge	Air cleaner

TABLE 1. 225 IN^3 INLINE 6 CYLINDER DIESEL ENGINE ENGINE SPECIFICATIONS (CONTINUATION)

Fuel metering systems:		
Type	.....	DB-2 - Distributor
Make	.....	Stanadyne
Exhaust gas recirculation system:		
Valve type	.....	Laboratory
Actuation	.....	Manual
Point of discharge	.....	Air cleaner
Exhaust system:		
Pipe diameter, inches nominal	.....	2.25

TABLE 2. CAR NUMBER 279 225 CID IN^3 INLINE 6, DIESEL VEHICLE SPECIFICATIONS

Model Year	1979
Make	Plymouth
Model	Volare
Body type	2 door sedan
Power plant*	225 in^3 inline 6 Diesel
Transmission:	
Type	Manual
Ratios, forward	3.09, 1.79, 1.00, 0.73
reverse	3.00
Axle:	
Ratio	2.76:1
Gear diameter, inches	7.25
Tire size	ER78 X 14 Glass
Fuel tank capacity, gallons	18
Accessories, engine load effective	None
Inertia weight class, as tested, lbs	3500
Horsepower load setting, hp	12.3

*See Table 1 for details.

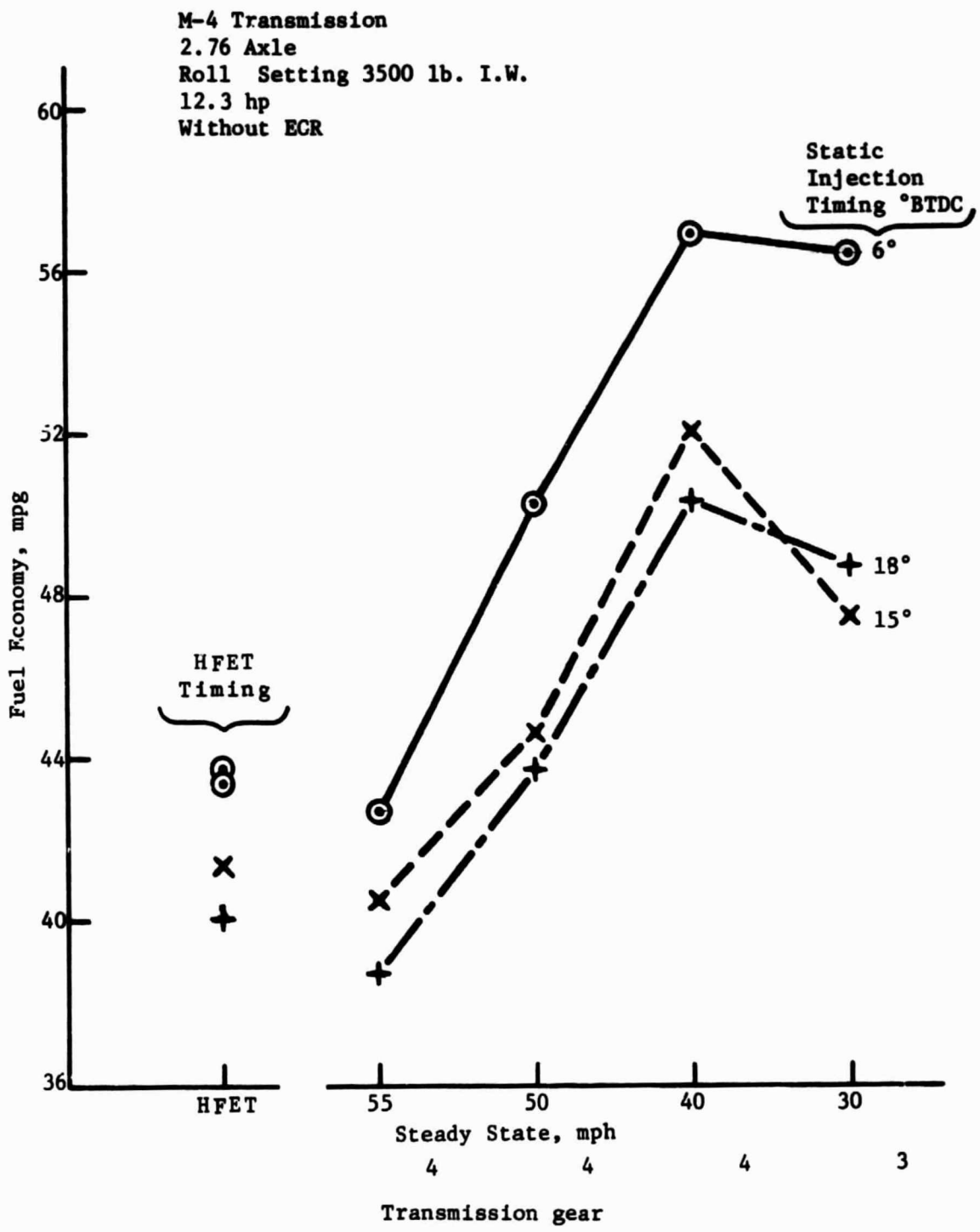

FIGURE 2. MANUFACTURER'S DATA, HIGHWAY FUEL ECONOMY TEST (HFET) AND STEADY STATE

to be used for particulate measurements. The analysis of this fuel is given in Table 3.

2.2 TEST EQUIPMENT

This section briefly describes the test equipment and the gaseous and particulate measurement techniques.

2.2.1 Dynamometer

The DOT/TSC chassis dynamometer is a fully programmable direct-current machine with a single 50-inch diameter roll. The features of this dynamometer are shown in Table 4. This dynamometer can simulate, individually and in combination, loads due to rolling losses, aerodynamic drag, vehicle inertia, uphill and downhill grades, as well as road-speed air-flow. Test cell temperature is normally controlled at 77° ± 5°F. Vehicle inertia can be simulated electrically or mechanically via flywheels. For the tests conducted here, electrical simulation of inertia was used.

The road-load horsepower setting for the vehicle was determined on the road (Figure 3) by coasting-down the vehicle from 60 mph using SAE Approved Practice J1263, "Road Load Measurement and Dynamometer Simulation Using Coast-Down Techniques". In the case of the programmable TSC dynamometer, the road-load was set over the complete speed profile (0-50 mph) and not just at the 50 mph point (Figure 4). The road-load horsepower at 50 mph measured in this manner, was 10.5 hp. Chrysler, in their tests, used 12.3 hp at 50 mph.

2.2.2 Gaseous Emissions Measurements

All measurements of gaseous hydrocarbons (HC), carbon monoxide (CO), nitrogen oxides (NO_x), and carbon dioxide (CO_2), were performed using a 325 cfm Constant Volume Sampling (CVS), with a Critical Flow Orifice (CFO) (Figure 5). For all tests, the gas samples (except HC) were collected in Tedlar bags. The instrumentation and procedures employed are those designated by EPA.[3] The

TABLE 3. DOE/BETC FUEL ANALYSIS

METHODS OF TESTS:

1. Hydrogen/Carbon - calculation based on atomic weight.
2. Specific gravity - ASTM D1298-67.
3. Heating Value - ASTM D240-76.
4. Hydrogen % - Pregl modified Ingram technique.
5. Carbon % - Pregl modified Ingram technique.
6. Sulfur % - ASTM D1552-64.
7. Cetane Index - ASTM D976-66.
8. Distillation - ASTM D86.
9. Aromatics, olefins and paraffins - ASTM D2789-71.

RESULTS:

Hydrogen/Carbon Calculation Based on atomic weight	1.73
Specific Gravity	0.8499
BTU per pound	19,594
BTU per gallon	138,647
Hydrogen, %	12.62
Carbon, %	86.97
Sulfur, %	0.19
Distillation, °F	
IBP	303
10%	401
50%	406
90%	584
End Point	637
Recovery, %	98.5
Cetane Index	48.2
Aromatics, %	24.7
Olefins, %	0.1
Paraffins, %	24.4

TABLE 4. DIRECT CURRENT CHASSIS DYNAMOMETER

- SINGLE AXIS, LARGE (50-INCH DIAMETER) ROLL (400 REVOLUTIONS/MILE)
- MAXIMUM TORQUE, SPEED: 6400 LB-FT, 0-39 MPH
- MAXIMUM POWER, SPEED: 315 HP, 39-105 MPH
- TORQUE SENSITIVITY: ±1.3 LB-FT (0.02% FULL SCALE)
- CORRESPONDING TRACTIVE FORCE AT WHEELS: ±0.61 LB
- DUAL TORQUE LOAD CELLS, 150% AND 15% OF FULL SCALE
- SIMULATED ROAD-SPEED AIR FLOW: 0-72 MPH
- MAXIMUM DRIVE-AXLE LOAD CAPACITY: 5000 LB
- MECHANICAL INERTIA OF SYSTEM EQUIVALENT TO VEHICLE WEIGHT OF 1800 LB
- ELECTRICAL SIMULATION OF VEHICLE WEIGHT FROM 1200 LB TO 7000 LB
- MECHANICAL SIMULATION OF VEHICLE WEIGHT FROM 1800 LB TO 8750 LB
- DIGITAL TORQUE CONTROL SYSTEM, PROGRAMMABLE TO SIMULATE:
  - ROLLING AND AERODYNAMIC LOSSES
  - VEHICLE INERTIA
  - POSITIVE AND NEGATIVE GRADES
  - HEAD AND TAIL WINDS
- ADJUSTABLE CONSTANT-SPEED CONTROL
- FULL DRIVE-CYCLE CAPABILITY

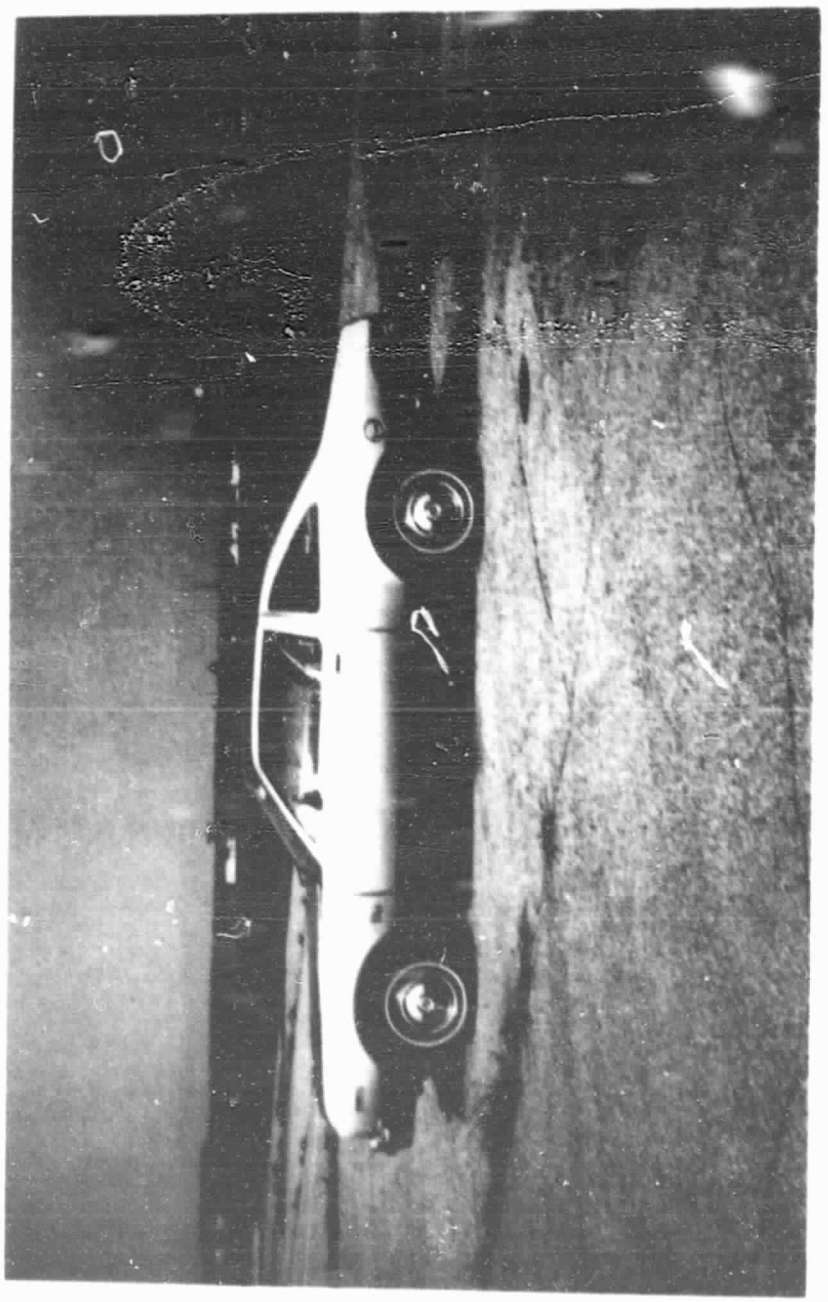

FIGURE 3. DETERMINING ROAD LOAD HORSEPOWER SETTING

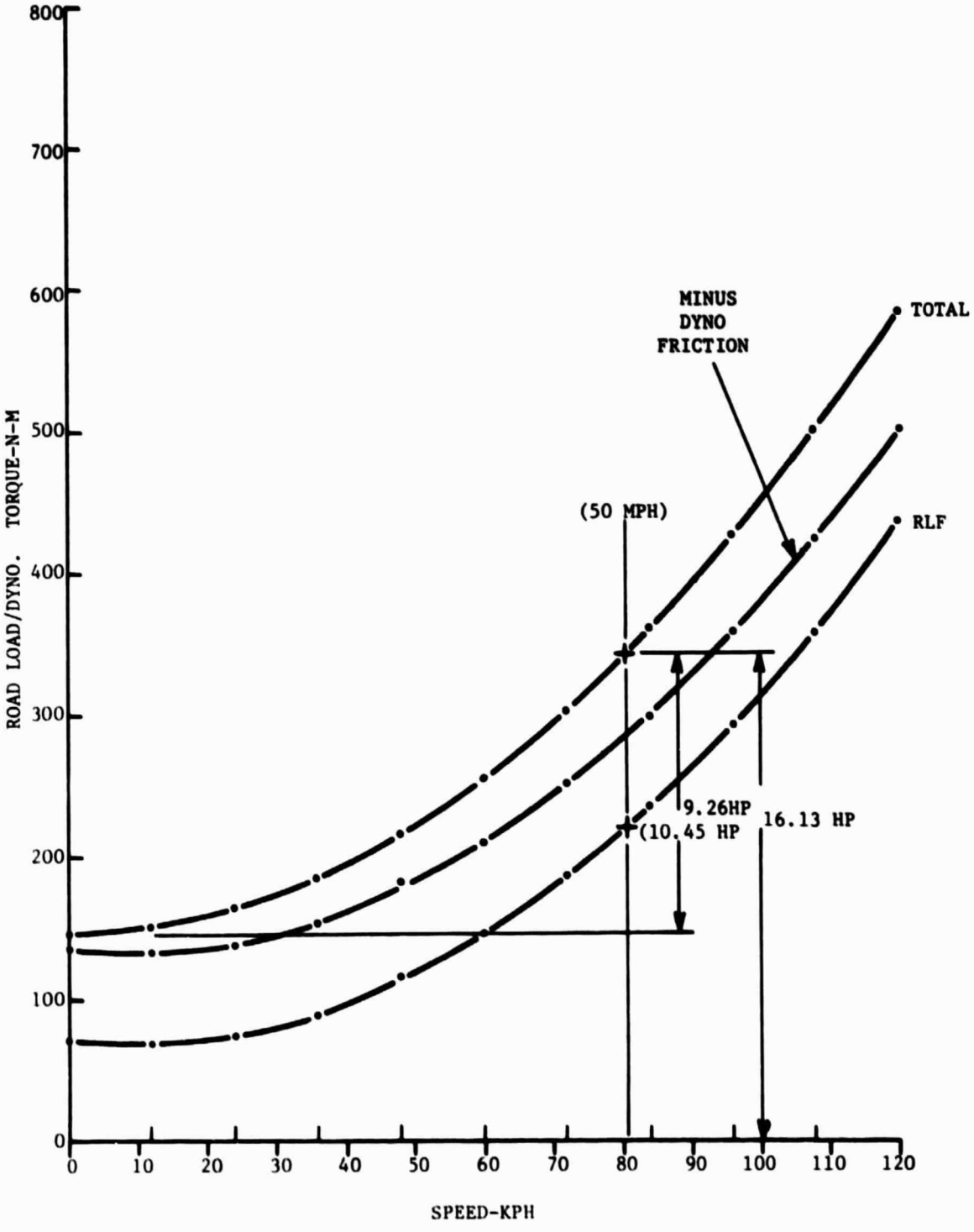

FIGURE 4. VOLARE DIESEL COAST-DOWN DATA

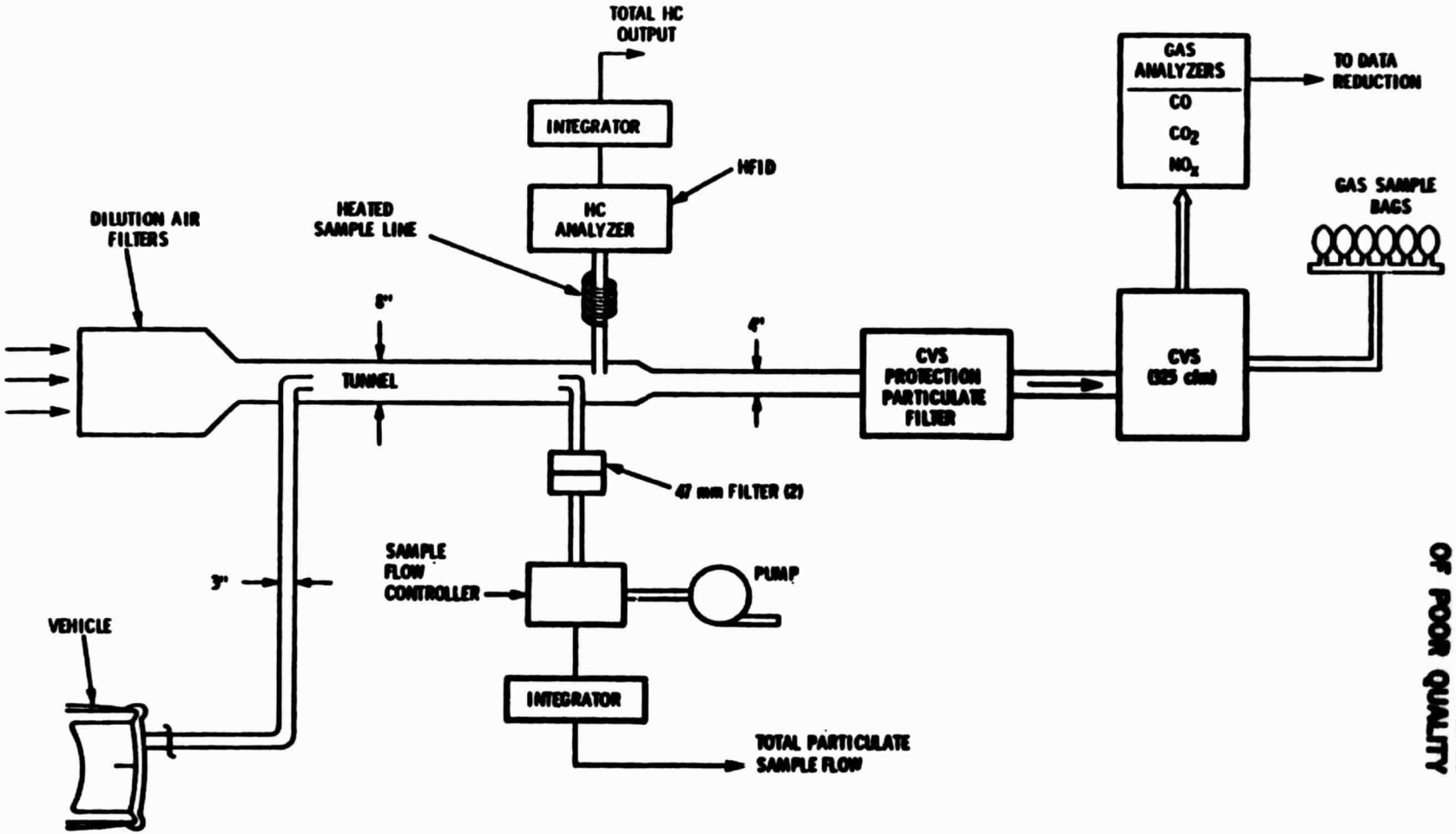

ORIGINAL PAGE IS
OF POOR QUALITY

FIGURE 5. AUTOMOTIVE RESEARCH LABORATORY PARTICULATE/GAS SAMPLING SYSTEM (CHARACTERIZATION)

instrumentation included non-dispersive infrared (NDIR) analyzers for CO and CO_2, a chemiluminescence analyzer with converter for NO_x, and a heated flame ionization detector (FID) for hydrocarbons (Table 5). For further detail regarding test procedures and instrumentation please refer to the Fiat 131 NA Report.[4]

2.2.3 Particulate Emission Measurement

Particulate mass measurements were performed using a dilution tunnel and the EPA recommended procedures for light-duty diesel vehicles.[5] The 8-inch diameter tunnel and its associated hardware are shown schematically in Figure 5. Tunnel specifications are listed in Table 6; particulate sampling instrumentation is indicated in Table 7.

To determine particulate mass (grams per mile), a sample of the diluted exhaust was extracted from the bulk-stream tunnel flow at a point which was 11 tunnel diameters downstream of the vehicle exhaust injection. The particulate sample probes (two each) were 1-inch diameter stainless-steel. The filter medium used was a 47-mm Pallflex T60A20 Teflon-coated fiberglass element held in Millipore model I quick-release holders.

For the substantial amounts of particulate matter needed for the DOE Diesel Health Effects Research Study, 20-inch x 20-inch Pallflex type T60A20 filters were used. These filters were mounted in parallel in two filter holders (Figure 6)that sampled approximately 25% of the exhaust stream after the dilution tunnel. All large and small filters were stored in a temperature and humidity controlled room prior to sample collection. After collections, the filters were allowed to stabilize in the weighing room prior to reweighing. After weighing, filters were placed in Tedlar envelopes and placed in dark freezer storage (approximately -20°C) as is recommended by EPA/RTP.

TABLE 5. GASEOUS EXHAUST EMISSION INSTRUMENTATION

Exhaust Species	Method	Model Number
Hydrocarbon	Heated Flame Ionization Detector	Scott 215 Beckman 402
Carbon Monoxide	Non-Dispersive Infrared (NDIR)	Horiba A1A-21 (AS) low range MSA 202 high range
Nitrogen Oxides	Chemiluminescence with Thermal Converter	Scott 125
Carbon Dioxide	NDIR	MSA 202
Oxygen	Paramagnetic	Beckman
Calibration Gases:	± 2% National Bureau of Standards Traceable.	

TABLE 6. EXHAUST DILUTION TUNNEL SPECIFICATIONS

Diameter	8 inches
Minimum Active Length*	75 inches
Minimum Residence Time	0.42 sec. @325 cfm
Material	Stainless Steel
Air Filters	
Prefilter	Cambridge Model 3CP60
Hydrocarbon Filter	Cambridge Activated Carbon Model 5FB45
Absolute Filter	Cambridge Model 1B-1000-1
Connecting Tubing - vehicle to tunnel	3-inch stainless steel smooth wall and silastic flexible couplings
Connecting Tubing - tunnel to CVS	4-inch flexible stainless steel and marmon couplings

*Distance From Vehicle Exhaust Exit To Nearest Sampling Port.

TABLE 7. EXHAUST PARTICULATE SAMPLING AND MEASUREMENT

Characterization	
Sample Probes	1 in. diam. stainless steel
Filter Holder	Millipore 47 mm
Filter Medium	Pallflex T60A20 Fluoropore
Sample Flow Control	Tylan Mass Flow Controller Model FC202 and FMT-3 electronics unit Model FMT-3 Integrator
Scale	Cahn Electrobalance, Model G
Large Volume Collection	
Filter Media	Pallflex T60A20 20" x 20"
Sample Flow Control	PDP pumped sample of approx. 100 cfm
Scale	Mettler P1200 (Modified)

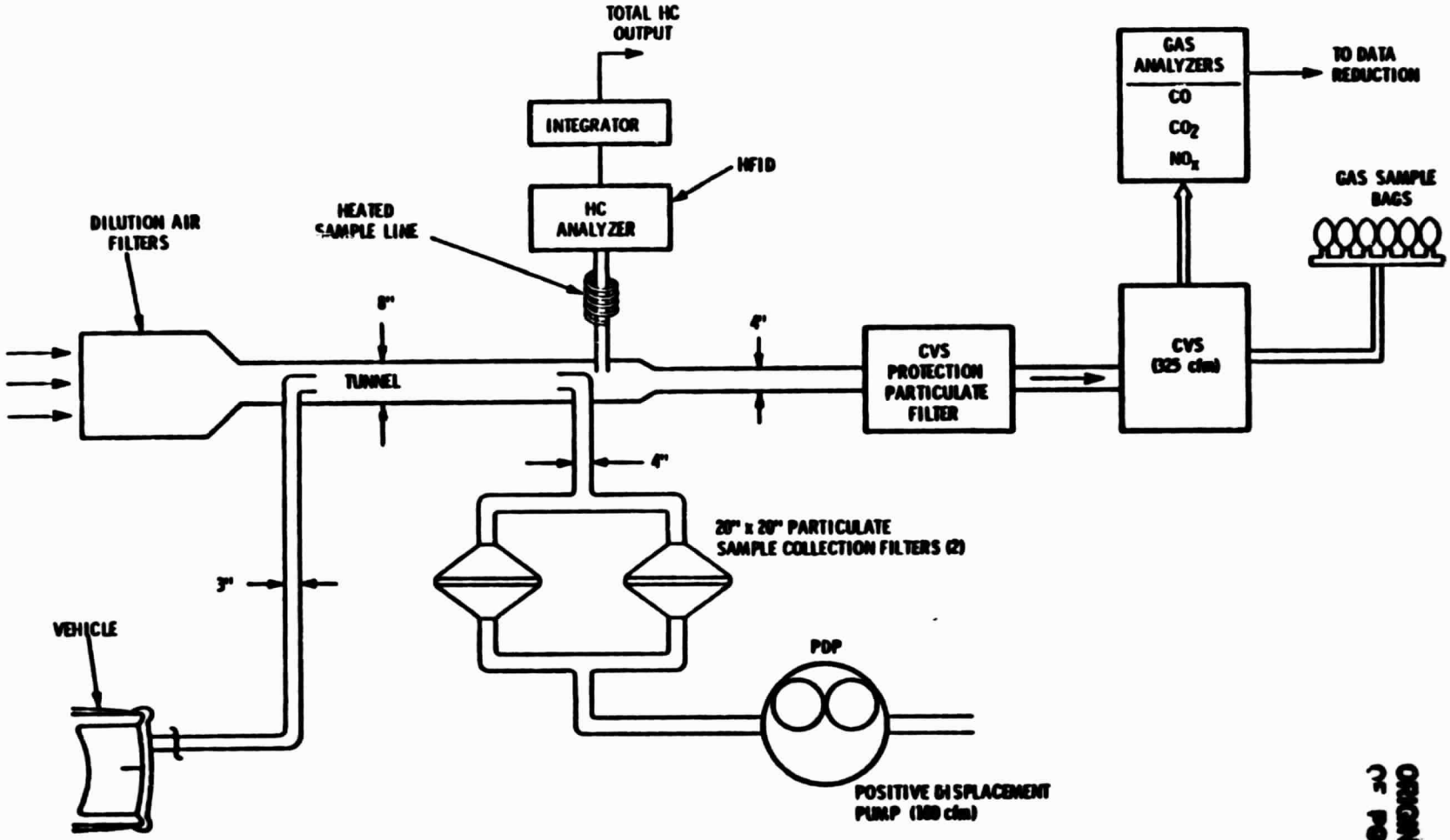

FIGURE 6. AUTOMOTIVE RESEARCH LABORATORY PARTICULATE/GAS SAMPLING SYSTEM (LARGE SCALE PARTICULATE COLLECTION)

3. TEST PROCEDURES

The laboratory test procedures used for determining the gaseous and particulate emissions rates and the fuel economy of the Chrysler Volare are those described in the Code of Federal Regulations.[6] For further detail refer to the Code or the Fiat 131 NA Report.[7] Two types of tests were conducted:

- o Characterization tests from which the gaseous and particulate exhaust emission rates and fuel economy were determined, and
- o Large-volume sampling tests during which large amounts of diesel exhaust particulates were collected on 20-inch x 20-inch filters for chemical and biological analyses.

The characterization tests employed the Federal Test Procedure Urban Cycle (FTP), the Highway Fuel Economy Test (HFET), and the New York City Cycle (NYCC) in addition to the steady-state speeds of 15 mph in second gear, 25 mph in second gear, 30 mph in third gear, 40 mph in third and fourth gear and 50 mph in third and fourth gear, 55 mph in fourth, and 60 mph in fourth gear. The large-volume sampling test involved only cyclic tests. Table 8 summarizes the characteristics of the three transient test cycles. Shift points are made according to the manufacturer's recommendation;

1st to 2nd gear....@	15 mph
2nd to 3rd gear....@	25 mph
3rd to 4th gear....@	40 mph.

TABLE 8. DRIVE CYCLE CHARACTERISTICS

	Distance (miles)	Avg. Speed (mph)	Time (sec)	Remarks
Federal Test Procedure (FTP)	11.1	21.6	1877	Composite
- Bag 1	3.6	25.6	505	Cold Start
- Bag 2	3.9	16.2	867	Stabilized
- Bag 3	3.6	25.6	505	Hot Start
Highway Fuel Economy Test (HFET)	10.2	48.2	765	
New York City Cycle (NYCC)	1.1	6.6	598	

4. RESULTS

4.1 GENERAL

The Chrysler Volare diesel exhibited good overall performance. Periodically, some stalling problems were encountered during the initial accelerations of the cold-start FTP. No explanation was apparent for these periodic problems. According to Chrysler, the vehicle static injection timing was set at 7° BTDC. This setting would give the optimized fuel economy. Chrysler measured the fuel economy, HC emissions, and NO_x emissions of the vehicle as a function of the injection timing using the 1974 "hot" FTP cycle. These results are shown in Figures 7, 8, and 9. Chrysler also measured the highway fuel economy (HFET) and steady-state fuel economy at four speed/gear combinations and at three injection timings (6°, 15° & 18° BTDC). These results are shown in Figure 2.

4.2 OVERALL RESULTS

According to the results reported here (Figure 10) the Chrysler could not meet the 1981 Federal Emission Standards of 0.41/3.4/1.0 g/mi of HC/CO/NO_x respectively. The Chrysler Volare diesel had g/mi emissions of 0.42/1.58/1.17 of HC/CO/NO_x. EPA may grant a waiver for new technology to 1.5 g/mi of NO_x. However, prototype vehicles must be designed to approximately 20 percent below regulated emission levels to account for production variability. The Chrysler Volare could meet the 1982 particulate emission standard of 0.6 gm/mile, but could not meet the proposed 1985 particulate standard of 0.2 gm/mile. (Note: all standards are currently up for review during 1982 Congressional action on the Clean Air Acts.) probably be made less stringent.)

Numerical tables of the results are included in Appendix A. Figures 10 through 12 are bar graphs of the emissions and fuel economy for each test. Emissions and fuel economy were heavily dependent on the drive cycle characteristics (See Table 8). For

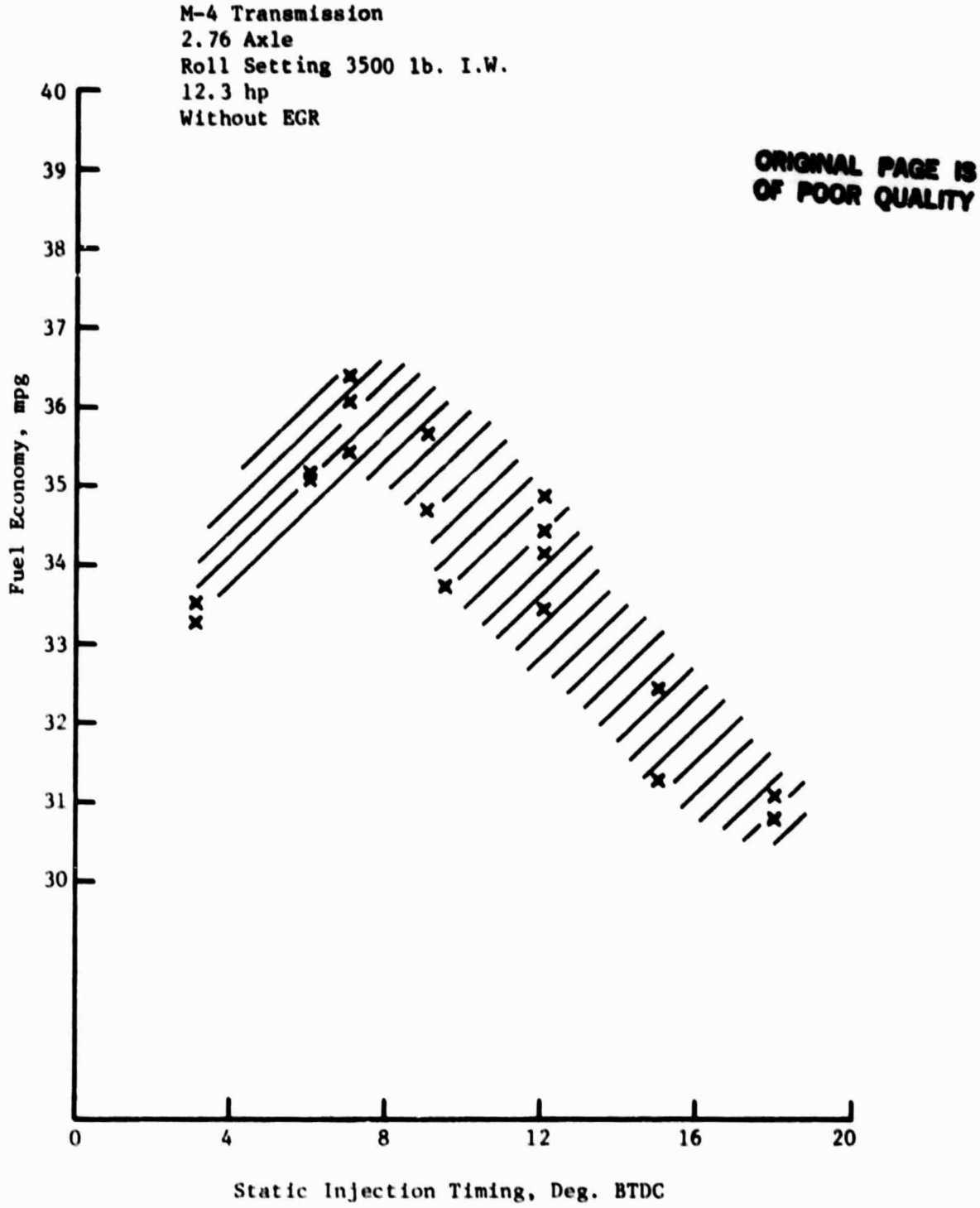

FIGURE 7. FUEL ECONOMY TESTS

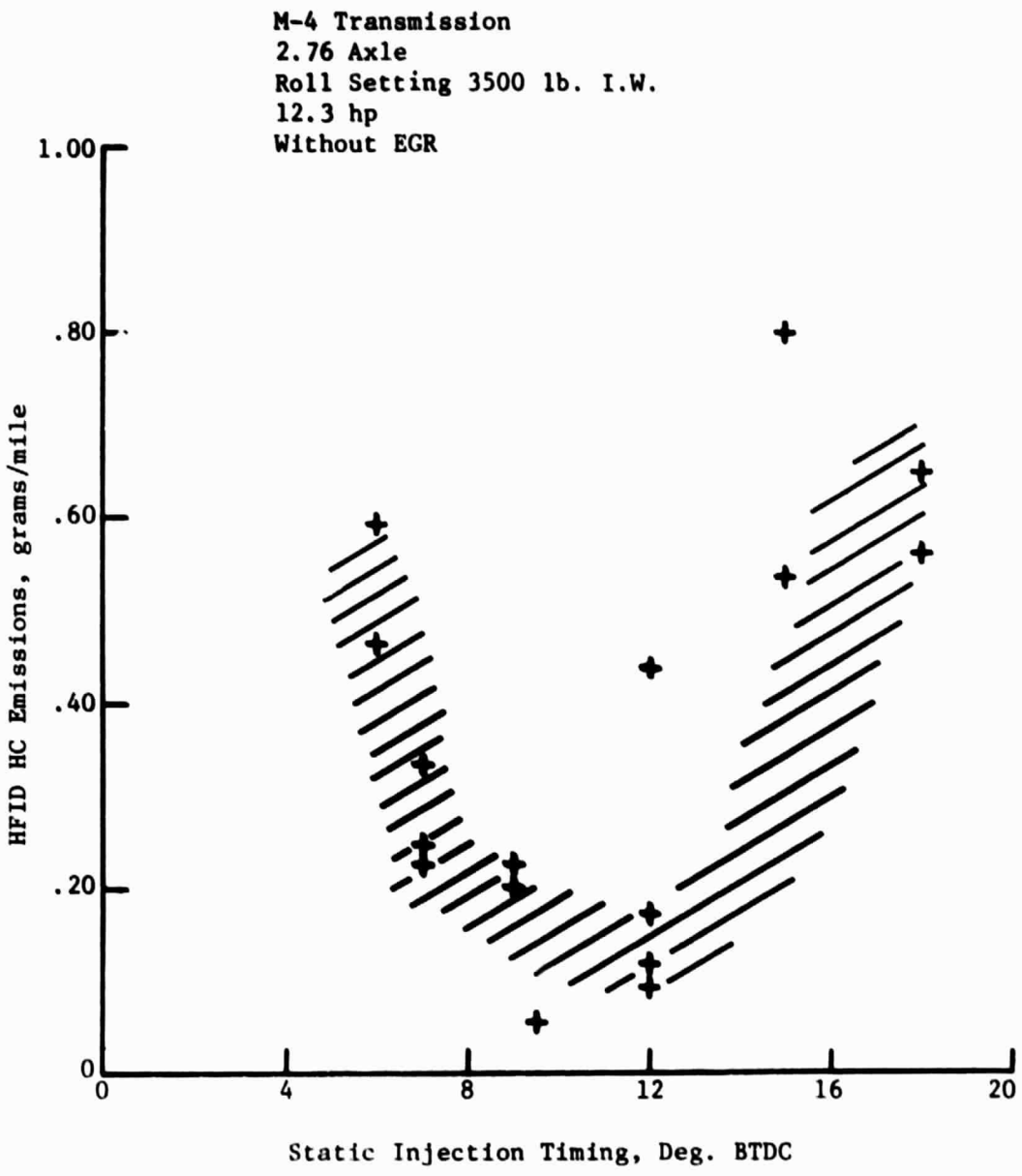

FIGURE 8. HYDROCARBON EMISSIONS

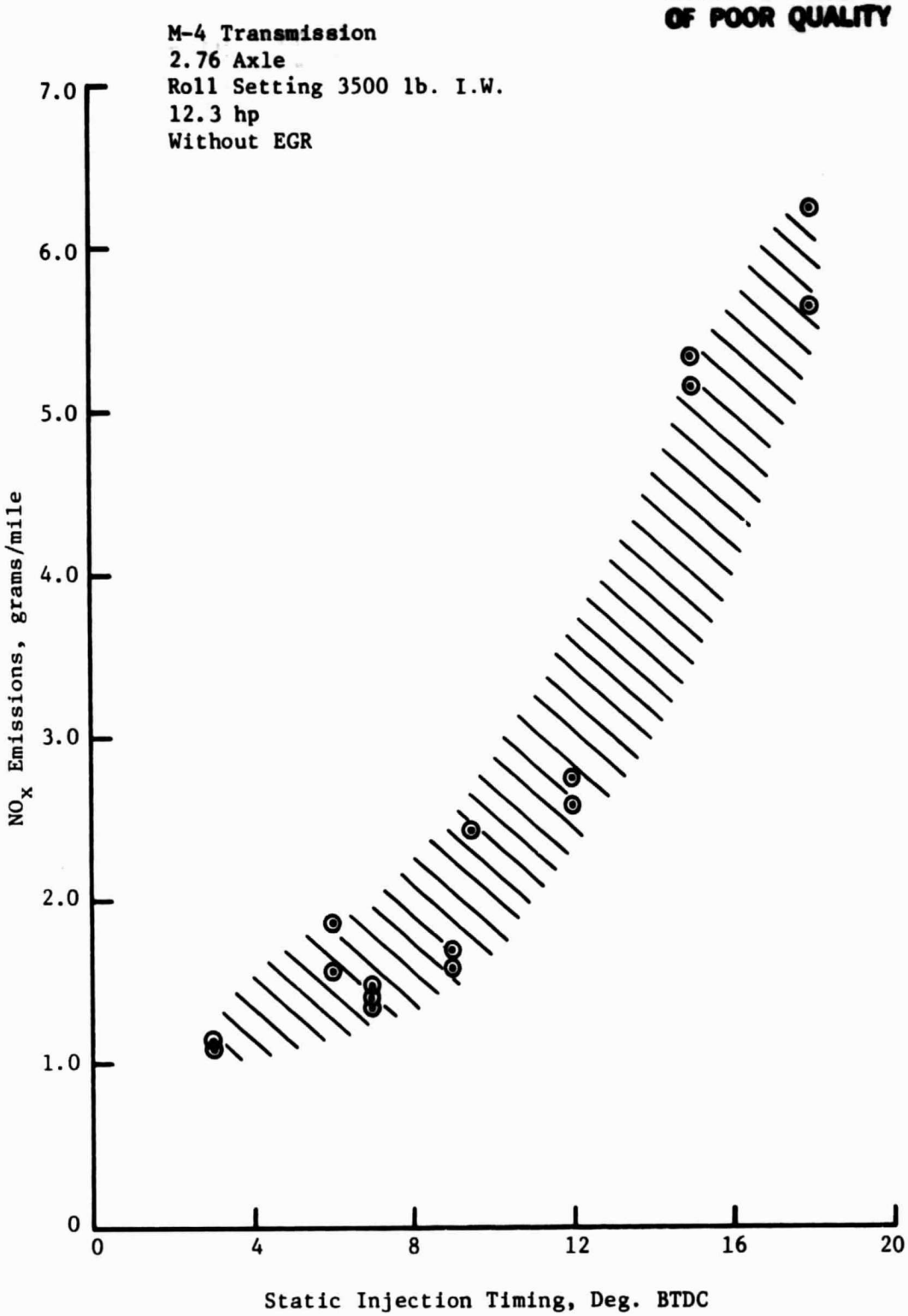

FIGURE 9. NOx EMISSIONS

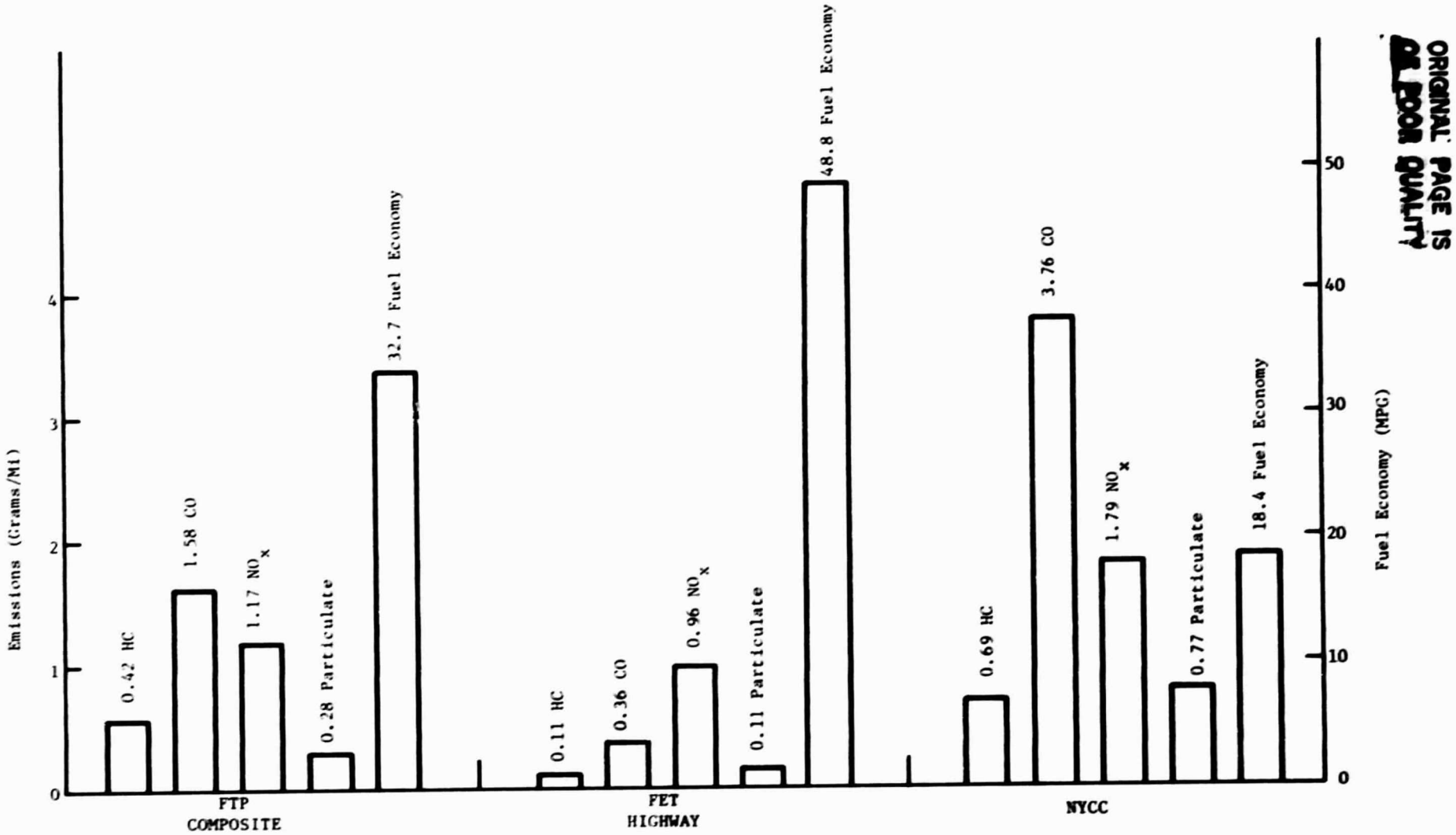

FIGURE 10. EMISSIONS AND FUEL ECONOMY OF A CHRYSLER VOLARE DIESEL CYCLIC TESTS

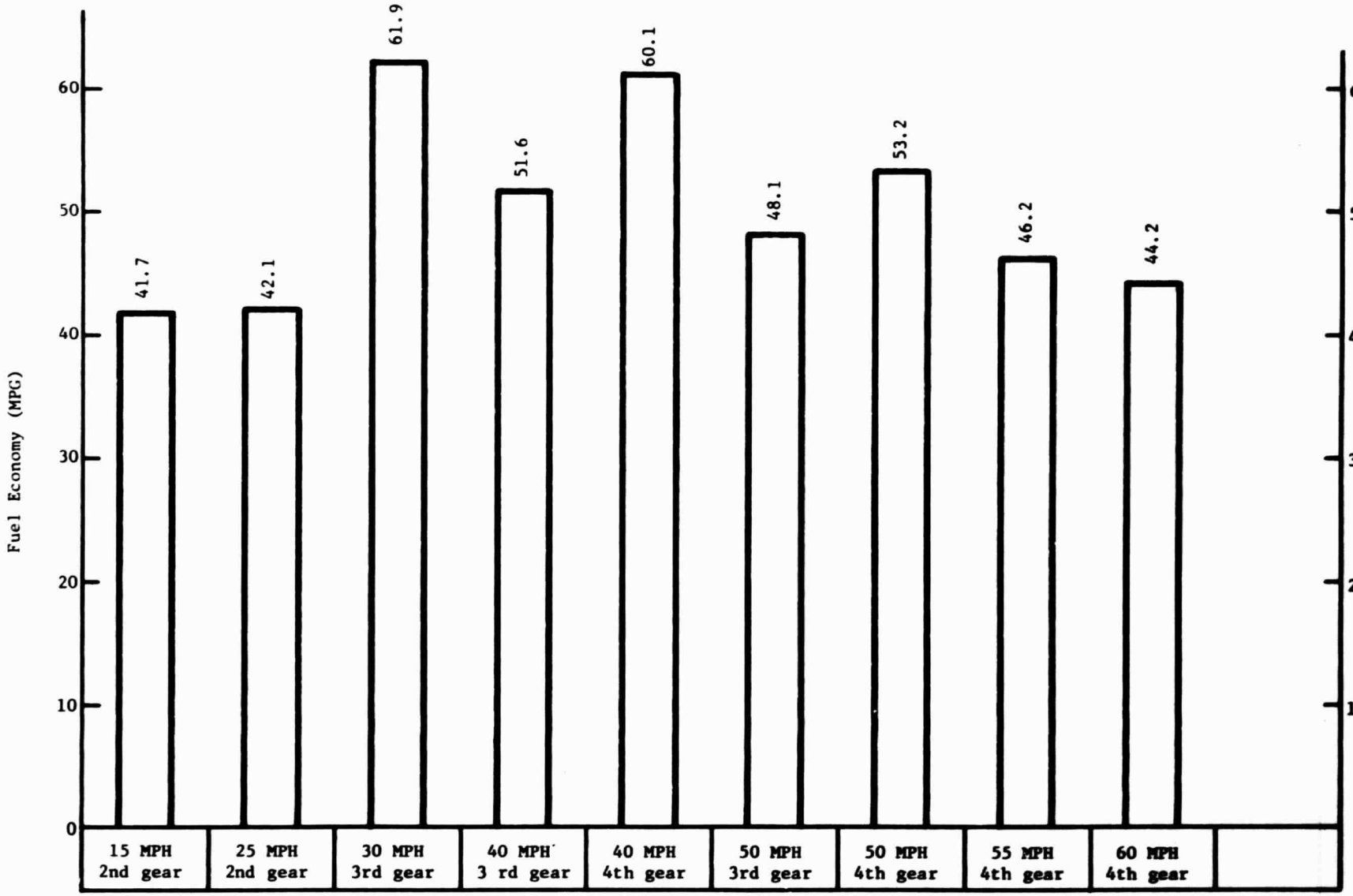

FIGURE 11. FUEL ECONOMY OF A CHRYSLER VOLARE DIESEL STEADY STATES

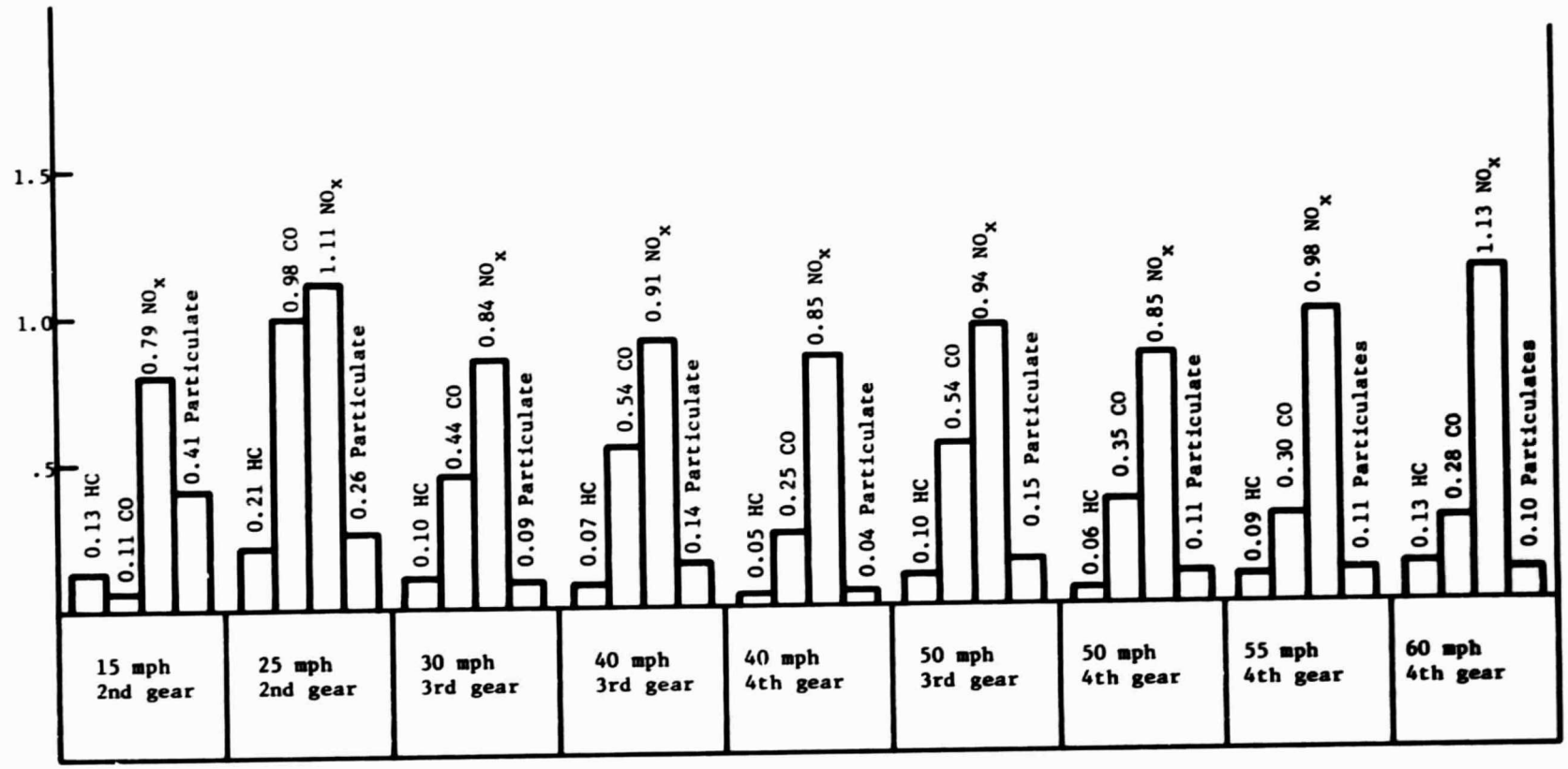

FIGURE 12. EMISSIONS OF A CHRYSLER VOLARE DIESEL STEADY STATES

example, the average speed of the NYCC is 6.6 mph and the measured fuel economy was 18.4 mpg, with emissions rates of 0.69/3.76/1.79/0.77 for HC/CO/NO_x and particulates, g/mile respectively. On the other hand, the average speed of the FET highway cycle is 48.2 mph and the Chrysler Volare diesel measured 48.8 mpg over this cycle.

Emission rates and fuel economy are temperature dependent as is evident by a comparison of the FTP bag 1 cold-start transient cycle, to bag 3 hot-start transient cycle. (See Appendix A). Hydrocarbons, carbon monoxide, and particulates decrease significantly from bag 1 to bag 3 whereas fuel economy increases by 18 percent. This temperature dependence is evident in a comparison of the Chrysler data using the "hot" 1974 Urban cycle (Figure 7) and TSC's data using the FTP cycle (Figure 10).The Chrysler fuel economy results are approximately 4 mpg higher then the TSC results even though the TSC dynamometer loading was 1.8 hp less at 50 mph (10.5 vs 12.3). The effect of the dynamometer loading is evident in the FET highway tests and the higher speed steady state tests where the TSC-measured fuel economy is approximately 10 percent higher than those measured by Chrysler.

4.2.1 Emissions

The hydrocarbons varied from a high of 0.69 gm/mile with the NYCC to 0.05 gm/mile at 40 mph in 4th gear. Carbon monoxide was highest for the NYCC (3.76 gm/mile) and lowest at the 15 mph in 2nd gear steady-state condition (0.11 gm/mile). Oxides of nitrogen were again highest in the NYCC (1.8 gm/mile) and lowest at 30 mph in 3rd gear (0.84 g/mile). Oxides of nitrogen emissions were the least sensitive to the test condition. Particulate emissions varied from 0.77 g/mile for the NYCC to 0.09 gm/mile at 30 mph in 3rd gear.

4.2.2 Fuel Economy

The measured fuel economy of the Chrysler Volare for the FTP urban cycle was 32.7 mpg. The highway fuel economy (FET) was

48.8 mpg. The best fuel economy was measured at 30 mph in 3rd gear, 61.9 mpg. Chrysler states that the Volare vehicle was built to demonstrate the best possible fuel economy, and that the urban milage obtained with this vehicle is evidence of levels that can be achieved with this diesel engine. A similar vehicle with automatic transmission, a higher rear axle ratio, and increased accessory loads was also tested by Chrysler. The "hot" urban cycle fuel economy test results from Chrysler for this vehicle was 26.5 mpg.

5. CONCLUSIONS

The dieselized version of the Chrysler "slant 6" engine performed well during these tests except for stalling problems encountered during accelerations of the cold-start FTP. This NA engine provided adequate power and acceleration. The fuel economy with the four-speed standard shift vehicle and 2.76:1 rear-axle ratio was extremely good for a 3500 lb test vehicle. Although the Volare could not meet 1981 emission standards, especially when considering production variability, some engine design changes could be used to improve performance and emissions. These changes include:

1) EGR for NO_x control,
2) Turbocharging with fuel system modifications for increased performance and, reduced emissions,
3) Improved fuel-injection system or electronic fuel injection control for HC and CO control.

The particulate level over the FTP cycle for the Chrysler Volare was low (0.28 gm/mile). However, in order to meet the proposed 1985 particulate level of 0.2 gm/mile, exhaust after-treatment may be required.

Chrysler, has studied the effects of EGR, turbocharging, and fuel system changes on fuel economy and emissions. Using engine maps and computer simulations, they studied the various fuel economy/emissions trade-offs for various emission control strategies. The reader can contact the author at the Transportation Systems Center, to learn when the report of these Chrysler studies will be available.

REFERENCES

1. S.S.Quayles, M.M.Davis, and R.A.Walter, "Fuel Economy and Exhaust Emissions Characteristics of Diesel Vehicles: Test Results of a Prototypes Fiat 131 NA 2.4 Liter Automobile," Report No. DOE/NASA/2817-1, Hereafter cited as Fiat 131 NA Report.
2. S.S.Quayle, "Fuel Economy and Exhaust Emissions Characteristics of Diesel Vehicles: Test Results of a Prototype Fiat 131 TC 2.4 Liter Automobile." Report No. DOE/NASA/2817-2.
3. Part 86, "Control of Air Pollution from New Motor Vehicles: Certification and Test Procedures" Code of Federal Regulations Protection of the Environment, revised as of July 1, 1980, Hereafter cited as Code.
4. Fiat 131 NA Report (See #1 above).
5. CODE (see #3 above).
6. Ibid.
7. Fiat 131 NA Report (See #1 above).

APPENDIX A

TABLE A-1. LARGE VOLUME PARTICULATE SAMPLES

CYCLE		NET MASS (grams) DOE FUEL
FTP Urban		
	Bags 1 and 2	1.84
	Bags 3 and 4	0.89
HFET (Highway)		1.23
NYCC		0.84

TABLE A-2. EMISSIONS AND FUEL ECONOMY VOLARE DIESEL AVERAGES

EMISSIONS					
CYCLE	HC (g/mi)	CO (g/mi)	NO_x (g/mi)	PARTICULATE (g/mi)	FUEL ECONOMY (mpg)
FTP Bag 1	1.10	2.57	1.06	0.60	30.4
Bag 2	0.29	1.16	1.20	0.22	32.3
Bag 3	0.26	1.64	1.00	0.45	35.8
COMPOSITE	0.42	1.58	1.17	0.28	32.7
HIGHWAY	0.11	0.36	0.96	0.11	48.8
NYCC	0.69	3.76	1.79	0.77	18.4
15 MPH/2nd GEAR	0.13	0.11	0.79	0.41	41.7
24 MPH/2nd	0.21	0.98	1.11	0.26	42.1
30 MPH/3rd	0.10	0.44	0.84	0.09	61.9
40 MPH/3rd	0.07	0.54	0.91	0.14	51.6
40 MPH/4th	0.05	0.25	0.85	0.04	60.1
50 MPH/3rd	0.10	0.54	0.94	0.15	48.1
50 MPH/4th	0.06	0.34	0.85	0.11	53.2
55 MPH/4th	0.09	0.30	0.98	0.11	46.2
60 MPH/4th	0.13	0.28	1.13	0.10	44.2

TABLE A-3. EMISSONS AND FUEL ECONOMY VOLARE DIESEL FTP CYCLE

		GASEOUS EMISSIONS					
CYCLE		HC (g/mi)	CO (g/mi)	NO_x (g/mi)	PARTICULATE (g/mi)	FUEL ECONOMY (mpg)	RUN #
FTP	Bag 1	1.18	2.75		0.59	30.1	81-131/2-17
		0.89	2.73	0.99	—	30.8	81-132/2-18
		1.12	2.07	1.10	0.58	31.3	81-136/2-19
		—	2.54	1.08	0.59	29.9	81-145/2-20
		1.23	2.76	1.08	0.65	29.9	81-152/2-24
	Bag 2	0.28	1.11	1.01	0.21	—	81-131/2-17
		0.28	1.20	1.22	—	32.0	81-132/2-18
		0.31	1.13	1.29	0.21	32.8	81-136/2-19
		—	1.20	1.29	0.24	32.1	81-145/2-20
	Bag 3	0.22	1.52	0.80	0.38	35.7	81-131/2-17
		0.24	1.81	1.06	0.67	35.3	81-132/2-18
		—	1.31	1.09	0.33	37.4	81-145/2-20
		0.32	1.94	1.05	0.44	34.8	81-152/2-24

TABLE A-4. EMISSIONS AND FUEL ECONOMY VOLARE DIESEL ALL CYCLES

	GASEOUS EMISSIONS					
CYCLE	HC (g/mi)	CO (g/mi)	NO_x (g/mi)	PARTICULATE (g/mi)	FUEL ECONOMY (mpg)	RUN #
FTP COMPOSITE	0.45	1.56		0.34	—	81-131/2-17
	0.39	1.68	1.13	0.18	32.6	81-132/2-18
	—	1.49	1.20	0.33	32.8	81-145/2-150
HIGHWAY	0.12	0.35	0.96	0.10	48.5	81-133/2-18
	0.06	0.38	0.95	0.11	48.8	81-137/2-19
	0.15	0.36	0.96	0.11	49.2	81-138/2-19
NYCC	0.98	3.00	1.72	0.73	19.0	81-133N
	0.41	4.42	1.86	0.81	17.9	81-146

TABLE A-5. EMISSIONS AND FUEL ECONOMY VOLARE DIESEL STEADY STATE SPEEDS VARIOUS GEARS

	GASEOUS EMISSIONS					
CYCLE	HC (g/mi)	CO (g/mi)	NO_x (g/mi)	PARTICULATE (g/mi)	FUEL ECONOMY (mpg)	RUN #
15 MPH/2ND	0.09	0.93	0.80	0.40	42.9	81-129/2-14
	0.27	1.36	0.92	0.42	35.2	81-153/2-24
	0.24	1.04	0.66	—	47.0	81-159/2-24
25 MPH/2ND	0.21	0.95	1.13	0.26	41.9	81-130/2-14
	0.20	1.02	1.10	—	42.3	81-154/2-24
30 MPH/3RD	0.11	0.41	0.79	0.09	62.0	81-139/2-19
	0.09	0.47	0.83	—	65.0	81-155/2-24
	0.10	0.43	0.89	—	58.6	81-161/2-24
40 MPH/3RD	0.04	0.54	0.87	0.12	51.3	81-140/2-19
	0.11	0.54	0.95	0.17	52.0	81-156/2-24

TABLE A-5. EMISSIONS AND FUEL ECONOMY VOLARE DIESEL STEADY STATE SPEEDS, VARIOUS GEARS (CONT.)

	GASEOUS EMISSIONS					
CYCLE	HC (g/mi)	CO (g/mi)	NO_x (g/mi)	PARTICULATE (g/mi)	FUEL ECONOMY (mpg)	RUN #
40 MPH/4TH	0.03	0.22	0.88	0.03	59.8	81-141/2-19
	0.07	0.28	0.83	0.06	60.5	
50 MPH/4TH	0.06	0.36	0.88	0.08	52.2	81-142/2-19
	0.06	0.34	0.82	0.14	54.3	81-149
50 MPH/3RD	0.10	0.54	0.94	0.15	48.1	81-148
55 MPH/4TH	0.19	0.29	0.96	0.04	48.2	81-134/2-18
	0.07	0.32	1.00	0.06	46.2	81-143/2-19
	0.05	0.30	0.94	0.25	42.9	81-150/
	0.07	0.30	1.01	0.08	47.7	81-162/2-24
60 MPH/4TH	0.21	0.27	1.10	—	44.4	81-135/2-18
	0.05	0.29	1.16	0.10	44.1	81-147

Ground State Energy of Electrons in a Static Point-Ion Lattice

D. F. Styer and N. W. Ashcroft

Laboratory of Atomic and Solid State Physics

Cornell University, Ithaca, New York 14853

We investigate the ground state energy of a neutral collection of protons and electrons, under the assumption that in the ground state configuration, static protons occupy the sites of a rigid Bravais lattice. We use the Wigner-Seitz method in conjunction with three postulated potentials: bare Coulomb, Thomas-Fermi screening, and screening by a uniform background charge. Within these approximations the exact band-minimum energy and wave function is derived. For each of the three potentials the approximate minimum ground state energy per proton (relative to isolated electrons and protons) is, respectively, -1.078 Ry, -1.038 Ry, and -1.052 Ry. These three minima all fall at a density of about 0.60 gm/cm^3, which is thus an approximate lower bound on the density of metallic hydrogen at its transition pressure.

MSC Report #4943

March 1983

I. INTRODUCTION

We wish to determine the ground state energy of N electrons in the presence of an equal number of infinitely massive neutralizing point charges. This by now standard problem was first considered from the band-theoretic point of view by Wigner and Huntington[1] in their investigation of the possibility of a high density metallic modification of hydrogen. In the intervening years, it has been treated by a variety of techniques,[2-4] some of them quite complex. Our purpose in this paper is to show that even within the simple, physically appealing framework of the Wigner-Seitz method (upon which the Wigner-Huntington paper was based) reliable ground state energies and accurate wave functions may be obtained with relatively little labor.

In the next section we formulate the N-electron, N-proton problem in order to establish the framework of the Wigner-Seitz calculation and to allow comparison with another common theoretical approach, namely the structural expansion. On the assumption that the effective one-body potential experienced by an electron is purely Coulombic, an exact solution of the Wigner-Seitz problem is given in Section III for the energy and wave function at the band minimum. This is developed further through a sequence of approximations (such as Bardeen's[5] effective mass theory) in order to estimate the total ground state energy. In Section IV we introduce a variational procedure to treat the case of screened Coulomb potentials. Finally, the results are discussed in Section V.

II. ELECTRONS IN A POINT-ION LATTICE

Consider a collection of N electrons and N protons confined in a volume Ω taken large enough that the system may be considered to be in the

thermodynamic limit. We focus entirely on electronic energies, and accordingly take the protons to be fixed at positions $\{\vec{R}_\ell\}$. If the electrons are assigned position and momentum operators $\{\hat{\vec{r}}_i\}$ and $\{\hat{\vec{p}}_i\}$, then the Hamiltonian for the system is

$$H = H_{ee} + H_{ep} + H_{pp} \tag{1}$$

where

$$H_{ee} = \sum_i \frac{\hat{\vec{p}}_i^{\,2}}{2m} + \frac{1}{2}\sum_{ij}{}' \frac{e^2}{|\hat{\vec{r}}_i - \hat{\vec{r}}_j|}, \tag{2a}$$

$$H_{pp} = \frac{1}{2}\sum_{\ell m}{}' \frac{e^2}{|\vec{R}_\ell - \vec{R}_m|}, \tag{2b}$$

and

$$H_{ep} = -\sum_{i\ell} \frac{e^2}{|\hat{\vec{r}}_i - \vec{R}_\ell|}. \tag{2c}$$

(Here m is an electron's mass and e the magnitude of its charge.)

The mean charge density of electrons in this system is $\rho = -eN/\Omega$, and the electrostatic energy of a uniform charge distribution with this density is $\frac{1}{2}\int_\Omega d\vec{r}d\vec{r}' \frac{\rho^2}{|\vec{r}-\vec{r}'|}$. The traditional interacting electron gas problem examines the energy of an electron system relative to this term, i.e., the corresponding Hamiltonian is taken to be

$$H_{eg} = \sum_i \frac{\hat{\vec{p}}_i^{\,2}}{2m} + \frac{1}{2}\sum_{ij}{}' \frac{e^2}{|\hat{\vec{r}}_i - \hat{\vec{r}}_j|} - \frac{1}{2}\int_\Omega d\vec{r}d\vec{r}' \frac{\rho^2}{|\vec{r}-\vec{r}'|}. \tag{3}$$

The ground state energy of H_{eg} has been studied extensively:[6,7] when expressed in terms of the linear density parameter $r_s = (3\Omega/4\pi N)^{1/3} a_0^{-1}$ (a_0 is the Bohr radius), it is approximately

$$NE^0_{eg}(r_s) = N\left(\frac{2.21}{r_s^2} - \frac{0.916}{r_s} - 0.115 + 0.031 \ln r_s\right)\text{Ry} \tag{4}$$

where the contributions are the familiar kinetic, exchange and correlation energy terms, the latter being the Nozières-Pines approximation (see below). Note also that in the large system limit, assumed here, H_{eg} may be written

$$H_{eg} = \sum_i \frac{\hat{\vec{p}}_i^{\,2}}{2m} + \frac{1}{2\Omega}\sum_{\vec{k}\neq 0} v_c(k)\hat{\rho}_e(k)\,\hat{\rho}_e(-\vec{k}) \tag{5}$$

where

$$v_c(k) \equiv 4\pi e^2/k^2 \tag{6}$$

and where

$$\hat{\rho}_e(\vec{k}) = \sum_i e^{i\vec{k}\cdot\hat{\vec{r}}_i} \tag{7}$$

is the one-particle density operator for electrons.

If we take $n(\vec{r})$ as the total charge density of the protons placed in a compensating uniform background of negative charge, i.e.,

$$n(\vec{r}) = \rho + e\sum_\ell \delta(\vec{r}-\vec{R}_\ell), \tag{8}$$

then (1) may be regrouped as

$$H = H_{eg} + \tag{9a}$$

$$+ \frac{1}{2} \int_{\Omega}' d\vec{r}d\vec{r}' \frac{n(\vec{r})n(\vec{r}')}{|\vec{r}-\vec{r}'|} \tag{9b}$$

$$- \sum_{\ell} \{ \sum_{i} \frac{e^2}{|\vec{r}_i - \vec{R}_\ell|} + \int_{\Omega} d\vec{r} \frac{\rho e}{|\vec{r}-\vec{R}_\ell|} \}. \tag{9c}$$

The term (9b) can now be recognized as the Madelung energy, $N E_M(r_s, \{\vec{R}_\ell\})$, for a static array of ions in a uniform compensating background. As indicated, E_M depends upon the density and upon the crystal structure of the proton lattice. However, the structural dependence is known to be weak,[8] and E_M may be accurately estimated using the spherical cell approximation in which each proton is surrounded by a sphere just large enough that the net charge within it vanishes (such a sphere has radius $r_s a_0$), and in which the overlap of spheres is ignored. This neutral sphere has electrostatic energy

$$E_M = \int_0^{r_s a_0} 4\pi r^2 dr \rho \left(1 - \left(\frac{r}{r_s a_0}\right)^3\right) \frac{e}{r} = -\frac{1.8}{r_s} \text{ Ry}, \tag{10}$$

which accurately approximates the structural result

$$E_M = \frac{1}{2\Omega N} \sum_{\vec{k}\neq 0} v_c(k) \hat{\rho}_p(\vec{k}) \hat{\rho}_p(-\vec{k}) \tag{11}$$

where

$$\hat{\rho}_p(\vec{k}) = \sum_{\ell} e^{i\vec{k}\cdot\vec{R}_\ell}. \tag{12}$$

(For crystalline lattices $\hat{\rho}_p(\vec{k}) = N \sum_{\ell} \delta_{\vec{k},\vec{K}_\ell}$ where $(\vec{K}_\ell)$ is the set of reciprocal lattice vectors.) Notice that the Madelung part of the Hamiltonian (i.e., 9b) may be rewritten exactly as

$$\frac{1}{2} N \int_{C_0} d\vec{r}d\vec{r}' \frac{n(\vec{r})n(\vec{r}')}{|\vec{r}-\vec{r}'|} + \frac{1}{2} \sum_{\ell,m}' \int_{C_\ell} d\vec{r} \int_{C_m} d\vec{r}' \frac{n(\vec{r})n(\vec{r}')}{|\vec{r}-\vec{r}'|} \tag{13}$$

where C_ℓ is the unit cell associated with site ℓ. The spherical cell approximation therefore calculates the Madelung energy by neglecting the last term of (13) and by replacing C_0 with a sphere of equal volume.

Next we examine (9c), which is the electron proton interaction energy relative to the interaction energy between protons and a uniform compensating background. We compare two methods for treating this term: first the structural expansion technique, which was applied to a point-ion system (metallic hydrogen) by Hammerberg and Ashcroft.[3] Second, the Wigner-Seitz method which is developed further here. To obtain the structural expansion we first recast (9) into the form

$$H = H_{eg} + NE_M - \frac{1}{\Omega} \sum_{\vec{k}\neq 0} v_c(k) \hat{\rho}_e(\vec{k}) \hat{\rho}_p(-\vec{k}), \tag{14}$$

which is valid in the thermodynamic limit. By introducing a coupling constant into the last term we may use a theorem of Pauli[9] to write the ground state energy as

$$ME^0(r_s,(\hat{R}_\ell)) = ME^0_{eg}(r_s) + ME_M(r_s,(\hat{R}_\ell))$$

$$- \frac{1}{\Omega} \sum_{\vec{k}\neq 0} v_c(k)\hat{\rho}_p(-\vec{k}) \int_0^1 \langle\lambda|\hat{\rho}_e(\vec{k})|\lambda\rangle d\lambda \qquad (15)$$

where $|\lambda\rangle$ represents the exact many electron ground state for H at coupling strength λ. Note that (9c) depends on structure through $\hat{\rho}_p(-\vec{k})$. The structural expansion calculates $\langle\lambda|\hat{\rho}_e(\vec{k})|\lambda\rangle$ by developing it in orders[10] of $v_c(k)\hat{\rho}_p(\vec{k})$. The linear term in response theory is

$$\langle\lambda|\hat{\rho}_e(\vec{k})|\lambda\rangle = \chi^{(1)}(\vec{k})\lambda\hat{\rho}_p(\vec{k})v_c(k) \qquad (16)$$

where $\chi^{(1)}(\vec{k})$ is the first order polarizability of the interacting electron gas. At this level of approximation

$$E^0 = E^0_{eg} + E_M - \frac{1}{2N\Omega} \sum_{\vec{k}\neq 0} v_c^2(k)\hat{\rho}_p(\vec{k})\hat{\rho}_p(-\vec{k})\chi^{(1)}(\vec{k}). \qquad (17)$$

Thus, the structural expansion explicitly uses the result (4) of the interacting electron gas problem, and its results may be systematically improved by applying higher orders of response theory.[3]

In contrast, the Wigner-Seitz[1] method involves approximations that are less well defined, and it cannot directly draw upon the standard electron gas result (4). However, it lends itself more readily to direct physical approximation: for example, it calculates approximate one-electron wave functions which are inaccessible via the structural expansion. (The

numerical results of the two methods are, in fact, quite similar.) In the Wigner-Seitz method, one first investigates approximate single-body wave functions $\phi_{\vec{k}}(\vec{r})$ by making an initial assumption (to be improved in Section IV) that when an electron's coordinate is found within the Wigner-Seitz cell of a given proton, the repulsion of the N-1 remaining electrons is exactly canceled by the attraction of the N-1 remaining protons. In this situation an electron is influenced only by its nearest neighbor proton and $\phi_{\vec{k}}(\vec{r})$ then satisfies the single-particle Schrödinger equation

$$\left(-\frac{\hbar^2}{2m}\nabla^2 - \frac{e^2}{r}\right)\phi_{\vec{k}}(\vec{r}) = E_{\vec{k}}\phi_{\vec{k}}(\vec{r}), \qquad (19)$$

where $\vec{r}$ may now be restricted to a single Wigner-Seitz cell. The boundary condition on this equation is most readily incorporated by invoking the spherical cell approximation, in which[11] the $\vec{k} = \vec{0}$ wave function is required to be spherically symmetric and satisfies

$$(d\phi_0(r)/dr)_{r=a_0} = 0. \qquad (20)$$

(When $\vec{k} \neq \vec{0}$, the appropriate boundary conditions are more complex,[5] but these conditions will not be needed in the following.) Thus the first step in the Wigner-Seitz calculation is to determine the $\vec{k} = \vec{0}$ "bottom of the band" energy by solving a radially symmetric one-body Schrödinger equation within the spherical unit cell. The total ground state energy for the full Hamiltonian (1) is then estimated using the techniques described in Section III.

III. TOTAL ENERGY: SPHERICAL CELL APPROXIMATION

If we possessed the N approximate one-electron wave functions, $\phi_{\vec{k}}(\vec{r})$, which are occupied in the ground state, then we could evaluate the exact Hamiltonian (1) in the Slater determinant constructed from these wave functions. The resulting Hartree-Fock-like approximation for the ground state energy is just

$$NE^0_{HF} = \frac{1}{N}\sum_{\vec{k},s}\int_\Omega d\vec{r}\,\phi^*_{\vec{k}}(\vec{r})\left(-\frac{\hbar^2}{2m}\nabla^2 - \sum_{\vec{R}_\ell}\frac{e^2}{|\vec{r}-\vec{R}_\ell|}\right)\phi_{\vec{k}}(\vec{r}) \tag{21a}$$

$$+\frac{1}{2N^2}\sum_{\vec{k},s}\sum_{\vec{k}',s'}\iint_{\Omega\Omega} d\vec{r}_1 d\vec{r}_2\,\frac{e^2}{|\vec{r}_1-\vec{r}_2|}\,|\phi_{\vec{k}}(\vec{r}_1)|^2|\phi_{\vec{k}'}(\vec{r}_2)|^2 \tag{21b}$$

$$-\frac{1}{2N^2}\sum_{\vec{k},s}\sum_{\vec{k}',s'}\iint_{\Omega\Omega} d\vec{r}_1 d\vec{r}_2\,\frac{e^2}{|\vec{r}_1-\vec{r}_2|}\,\delta_{s,s'}\phi^*_{\vec{k}}(\vec{r}_1)\phi_{\vec{k}}(\vec{r}_2)\phi^*_{\vec{k}'}(\vec{r}_2)\phi_{\vec{k}'}(\vec{r}_1) \tag{21c}$$

$$+\frac{1}{2}\sum_{\ell,m}{}'\,\frac{e^2}{|\vec{R}_\ell-\vec{R}_m|}\,. \tag{21d}$$

where the $\vec{k},s$ sums extend over the occupied levels (s represents the electron spin projection). We assume the wave functions are normalized by

$$\int_\Omega d\vec{r}\,|\phi_{\vec{k}}(\vec{r})|^2 = N \quad \text{or} \quad \int_{C_0} d\vec{r}\,|\phi_{\vec{k}}(\vec{r})|^2 = 1. \tag{22}$$

Each integral over the volume in (21a-b) may be broken into a sum over lattice sites m plus an integral over the corresponding Wigner-Seitz cell C_m. In the spherical cell approximation all of the "cross terms"

involving two different cells can be evaluated exactly, and they conspire to exactly cancel the proton-proton energy (21d). In addition, (19) may be used to simplify (21a), leading to

$$E^0_{HF}(r_s) = \frac{1}{N}\sum_{\vec{k},s} E_{\vec{k}} \tag{23a}$$

$$+\frac{1}{N^2}\sum_{\vec{k},s}\sum_{\vec{k}',s'}\frac{1}{2}\int_{C_0}\int_{C_0} d\vec{r}_1 d\vec{r}_2\,\frac{e^2}{|\vec{r}_1-\vec{r}_2|}\,|\phi_{\vec{k}}(\vec{r}_1)|^2|\phi_{\vec{k}'}(\vec{r}_2)|^2 \tag{23b}$$

$$-\frac{1}{2N^3}\sum_{\vec{k},s}\sum_{\vec{k}',s'}\iint_{\Omega\Omega} d\vec{r}_1 d\vec{r}_2\,\frac{e^2}{|\vec{r}_1-\vec{r}_2|}\,\delta_{s,s'}\phi^*_{\vec{k}}(\vec{r}_1)\phi_{\vec{k}}(\vec{r}_2)\phi^*_{\vec{k}'}(\vec{r}_2)\phi_{\vec{k}'}(\vec{r}_1) \tag{23c}$$

where the sums are understood to be over the occupied levels. We will treat each of the three components in turn.

First, we examine the average single-body energy, (23a). The first term in the sum is just E_0, the band minimum, which is found by solving the boundary value problem

$$-\frac{\hbar^2}{2m}\left(\frac{d^2}{dr^2}+\frac{2}{r}\frac{d}{dr}\right)\phi_0(r) - \frac{e^2}{r}\phi_0(r) = E_0\phi_0(r), \tag{24}$$

$$(d\phi_0/dr)_{r_s a_0} = 0. \tag{25}$$

Following Bardeen,[5] we make the substitutions $S = r\phi$, $\mathcal{E}_b = -\mathcal{E}_0/(e^2/2a_0)$ and $y = 2\mathcal{E}_b^{1/2} r/a_0$. The equation for S is then Whittaker's equation

$$\frac{d^2S}{dy^2} + [\frac{\mathcal{E}_b^{-1/2}}{y} - \frac{1}{4}]S = 0 \qquad (26)$$

which leads to the solution, regular at the origin,

$$\phi_0(y) = Ae^{-y/2}M(1 - \mathcal{E}_b^{-1/2};2;y) \qquad (27)$$

where M(a;b;y) is Kummer's confluent hypergeometric function.[12,13] Application of the boundary condition (25) then leads to the simple non-linear eigenvalue equation

$$(\frac{1}{2}y_s - 1 - \mathcal{E}_b^{-1/2})M(1 - \mathcal{E}_b^{-1/2};2;y_s) + (1 + \mathcal{E}_b^{-1/2})M(-\mathcal{E}_b^{-1/2};2;y_s) = 0. \qquad (28)$$

The binding energy $\mathcal{E}_b$ is easily found by solving (28) numerically: in the regime of interest Kummer's function may be evaluated to desired accuracy by simply retaining more and more terms of its power series representation. The normalized wave function for $r_s = 1.5$ is plotted in figure 1.

The wave function (27) has a cusp at the origin, as do all the hydrogen atom wave functions. In fact, all these cusps are identical in that

$$(d(\ln \phi)/dr)_{r=0} = -a_0^{-1}. \qquad (29)$$

This cusp condition has recently been proven to apply under very general conditions:[14] it will aid us in later calculations when no exact solution

is available.

We must now find the effect of the potential V(r) on $E_{\hat{k}}$ when $\hat{k} \neq \hat{0}$. These effects are manifested principally in an effective mass m^*, defined by

$$E_{\hat{k}} = E_0 + \frac{\hbar^2k^2}{2m^*} + O(k^3). \qquad (30)$$

(The higher order terms in k may be ignored because the band is only half filled.) Bardeen[5] has shown that m^* is given by

$$\frac{m}{m^*} = \frac{4}{3}\pi(r_s a_0)^3[\phi_0^2(r)(\frac{r}{P}\frac{dP}{dr} - 1)]_{r = r_s a_0} \qquad (31)$$

where the function P(r) is a solution of

$$\frac{d^2P}{dr^2} - \frac{2}{r^2}P + \frac{2m}{\hbar^2}(E_0 - V(r))P = 0. \qquad (32)$$

For a Coulomb potential we may use the variables introduced in (24) to write this equation as

$$\frac{d^2P}{dy^2} + [-\frac{1}{4} + \frac{\mathcal{E}_b^{-1/2}}{y} - \frac{2}{y^2}]P = 0, \qquad (33)$$

which is once again Whittaker's equation. The P(r) dependent quantity in (31) is given by

$$\left(\frac{r}{p}\frac{dp}{dr}\right)_{r_s a_0} = \left(\frac{\gamma_s}{2} - \xi_b^{-1/2}\right) + \left(2 + \xi_b^{-1/2}\right)\frac{M(1 - \xi_b^{-1/2};4;y_s)}{M(2 - \xi_b^{-1/2};4;y_s)} . \qquad (34)$$

Once m^* is thus obtained, we approximate (23a) by

$$\frac{1}{N}\sum_{k,s}^{*} E_k = E_0 + \left(\frac{m}{m^*}\frac{2.21}{r_s^2}\right)\text{Ry}. \qquad (35)$$

Now we investigate the Hartree energy (23b). The first term in the sum is

$$H_{00} \equiv \frac{e^2}{2}\int\int_{C_0 C_0} d\vec{r}_1 d\vec{r}_2 \frac{\phi_0^2(r_1)\phi_0^2(r_2)}{|\vec{r}_1 - \vec{r}_2|} = 16e^2\pi^2 \int_0^{r_s a_0} dr\, r\, \phi_0^2(r) \int_0^{r} dr' r'^2 \phi_0^2(r'). \qquad (36)$$

This term can be evaluated using the power series representation for Kummer's function, but convergence is slow enough that this is not practical for r_s greater than about 3.5. For larger values of r_s the integral is readily evaluated numerically. The remaining terms in the Hartree sum can also be evaluated, but only with considerable effort. This may be avoided, however, by noting that (36) is the largest term in the Hartree sum. This follows from the observation that the low energy $\vec{k} = \vec{0}$ wave function is itself much larger near the center of the cell (where potential energy is low) than at its edge, whereas the high energy wave functions are more uniform in amplitude. On the other hand, a lower bound on the sum is necessarily given by the Hartree integral for a flat

wave function, namely

$$16e^2\pi^2 \int_0^{r_s a_0} dr\, r \frac{3}{4\pi(r_s a_0)^3} \int_0^{r} dr' r'^2 \frac{3}{4\pi(r_s a_0)^3} = \frac{6}{5r_s}\text{Ry}. \qquad (37)$$

At $r_s = 1.5$, the upper bound (36) is only 5% larger than the lower bound (37). This fortunate numerical coincidence implies that little error is introduced by taking the sum (23b) as the average of the two bounds (36) and (37). This is precisely the approximation that we will employ.

The remaining exchange term (23c) is traditionally difficult to evaluate. Wigner and Huntington[1] argue that it is closely approximated by the uniform interacting electron gas result $-(0.916/r_s)$Ry, and we also accept this result.

Finally, E_{HF}^0 must be corrected by adding a correlation energy. We will again use a uniform electron gas result, namely the Nozières-Pines[7] interpolation formula $(-0.115 + 0.031 \ln r_s)$Ry. Our final approximation for the ground state energy per electron is thus

$$E^0(r_s) = E_0 + \left[\frac{m}{m^*}\frac{2.21}{r_s} + \frac{1}{2}\left(H_{00} + \frac{6}{5r_s}\right) - \frac{0.916}{r_s} - 0.115 + 0.031 \ln r_s\right]\text{Ry}, \qquad (38)$$

where H_{00} appears in (36). This result is plotted in figure 2: the zero pressure density corresponds to $r_s = 1.66$, at which point the cohesive energy (relative to well-separated electrons and protons) is -1.078 Ry. The results are numerically quite close to those of Chakravarty *et al.*,[2] which were obtained using a completely different method.

Because the Hamiltonian is explicitly spin-independent, the above discussion is readily extended to consider a spin polarized ground state. In this case the kinetic energy term $2.21/r_s^2$ becomes $3.51/r_s^2$, and the exchange term $-0.916/r_s$ becomes $-1.154/r_s$. Otherwise equation (38) is unchanged. These results are also graphed in figure 1: paramagnetic and spin aligned energies are seen to be equal at $r_s = 3.50$.

IV. SCREENING EFFECTS

In Section III we found approximate single-body wave functions from a Schrödinger equation which ignored electron-electron repulsion. Subsequently, the total energy was obtained by evaluating the exact Hamiltonian in a state constructed from these wave functions. Better wave functions, and more accurate energies, may be obtained by utilizing a screened potential. The Schrödinger equation then becomes (hereafter we use atomic units with $Ry = a_0 = e^2/2 = 1$)

$$\left(-\nabla^2 - \frac{2}{r} + U(\vec{r})\right) \phi_{\vec{k}}(\vec{r}) = E_{\vec{k}}\, \phi_{\vec{k}}(\vec{r}), \tag{39}$$

where $U(\vec{r})$ is some average potential arising from electron-electron repulsion. We now examine two such screening potentials: first the potential of a negative unit charge uniformly distributed throughout the Wigner-Seitz sphere, namely

$$U_B(\vec{r}) = \frac{1}{r_s^3}\left(3r_s^2 - r^2\right). \tag{40}$$

Second, a Thomas-Fermi screening potential

$$U_{TF}(r) = \frac{2}{r}\left(1 - e^{-k_{TF} r}\right), \quad k_{TF} = \left(\frac{12}{\pi}\right)^{1/3} \frac{1}{r_s^{1/2}}. \tag{41}$$

For the first case the $\vec{k} = \vec{0}$ Schrödinger equation can be solved exactly using the power series method. For the second the Schrödinger equation is analyzed variationally.

We begin by noting that the total Hamiltonian (1) can be trivially rewritten as:

$$H = H + \sum_{i,\ell} U(\vec{r}_i - \vec{R}_\ell) - \sum_{i,\ell} U(\vec{r}_i - \vec{R}_\ell), \tag{42}$$

where $U(\vec{r})$ is now chosen to vanish for $\vec{r}$ outside the Wigner-Seitz cell. By evaluating this Hamiltonian in a Slater determinant composed of solutions to (39), we find that the Hartree-Fock-like energy (23) is altered only by the addition of the (negative) term

$$-\frac{1}{N} \sum_{\vec{k},s} \int_0 d\vec{r}\, \left|\phi_{\vec{k}}(\vec{r})\right|^2 U(r). \tag{43}$$

This sum can be estimated (as the Hartree sum was), by averaging the lower bound

$$-4\pi \int_0^{r_s} r^2 dr\, \phi_0^2(r)\, U(r) \tag{44}$$

and the upper bound (obtained using unimodular wave functions in (43))

$$-\frac{4\pi}{\frac{4\pi r_s^3}{3}}\int_0^{r_s} r^2 dr\ U(r). \tag{45}$$

This last expression is equal to

$-12/(5r_s)$. (uniform background potential)

$$-\frac{6}{r_s^3}\left[\frac{r_s^2}{4} - \frac{1}{k_{TF}} + e^{-k_{TF}r_s}\left(\frac{r_s}{k_{TF}} + \frac{1}{k_{TF}^2}\right)\right].$$ (Thomas-Fermi potential).

As with the earlier Hartree sum, the loss of accuracy involved in this bounding procedure is not serious. Note that at $r_s = 1.5$ the two bounds differ by only 3% (for both potentials).

We will treat the uniform background potential first. The boundary value problem for $\phi_0(r)$ is then

$$\left[-\frac{d^2}{dr^2} - \frac{2}{r}\frac{d}{dr} - \frac{2}{r} + \frac{1}{r_s^3}(3r_s^2 - r^2)\right]\phi_0(r) = E_0\phi_0(r), \tag{46}$$

$$(d\phi_0/dr)_{r_s} = 0. \tag{47}$$

Although (46) is apparently not a "standard" or "named" differential equation, it is easily solved using the method of Frobinius.[15] Only one solution is regular at the origin, and it is

$$\phi_0(r) = \frac{A}{r}S(r) = \frac{A}{r}\sum_{l=0}^{\infty} s_l r^l. \tag{48}$$

where

$$s_0 = 0,\ s_1 = 1,\ s_2 = -1,\ s_3 = (1/6)(2-E_0 + 3/r_s)$$

$$s_l = -\frac{1}{l(l-1)}\left[2s_{l-1} + \left(E_0 - \frac{3}{r_s}\right)s_{l-2} + \frac{1}{r_s^3}s_{l-4}\right]. \quad l\geq 4 \tag{49}$$

The series for $S(r)$ converges absolutely and uniformly for all r, so we may interchange differentiation and summation. Hence boundary condition (47) becomes

$$\sum_{l=1}^{\infty}(l-1)\,s_l r_s^{\,l} = 0, \tag{50}$$

which leads to an eigenvalue equation for E_0, and which is easily solved numerically. Notice that the cusp condition (29) is exactly satisfied by wave function (48), despite the use of a non-Coulombic potential (see footnote 8 of reference 14).

The effective mass may be determined from equations (31) and (32), where now $V(r) = -2/r + U_0(r)$. The relevant solution of (32) is

$$P(r) = \sum_{i=0}^{\infty} p_i r^i; \qquad p_0 = p_1 = 0,\ p_2 = 1,\ p_3 = -1/2$$

$$p_i = \frac{-1}{i(i-1)-2}\left(2p_{i-1} + (E_0 - \frac{3}{r_s^3})p_{i-2} + \frac{1}{r_s^3}\,p_{i-4}\right). \qquad i \geq 4 \qquad (51)$$

Finally the Hartree, exchange, and correlation energies are treated as they were for a pure Coulomb potential. To the ground state energy formula (38) we must therefore add our estimate for the sum (43). The resulting energy estimate is plotted against r_s in figure 3. The minimum energy, $E^0 = -1.052$ Ry, falls at $r_s = 1.65$.

The analysis of the Thomas-Fermi potential may be approached using the same power series method. Indeed, we find that (49) is replaced by

$$s_0 = 0,\ s_1 = 1,\ s_i = -\frac{1}{i(i-1)}\left(2\sum_{m=0}^{i-1}\frac{(-k_{TF})^{i-m-1}}{(i-m-1)!}\,s_m + E_0\ s_{i-2}\right) \quad i \geq 2. \qquad (52)$$

The cusp condition is again satisfied exactly. However, because s_i depends upon <u>all</u> the preceding coefficients s_0 to s_{i-1}, we have not been able to establish that the series actually converges. Numerical evidence indicates that it does, in fact, converge, but only very slowly. For r_s greater than about 1.2, convergence is slow enough that the exact power series solution is of little help in practical calculations. These are physically important values of r_s, so a different approach is clearly required.

The variational method proves to be an accurate technique for finding E_0 and $\phi_0(r)$. A suitable trial wave function $\phi_t(r)$ must satisfy the

symmetry condition

$$\phi_t(r_s + \Delta) = \phi_t(r_s - \Delta). \qquad (53)$$

in order to assure that the boundary condition (20) is satisfied in such a way that the wave function is smooth at $r = r_s$. In addition, it is expected to behave like the 1s hydrogenic wave function near the origin, i.e.,

$$\phi_t(r) = A\,e^{-r} \text{ for } r \ll r_s. \qquad (54)$$

Both of these requirements are satisfied by the choice

$$\phi_t(r) = b_0 \cosh(r - r_s) + \sum_{n=1}^{M} b_n \sin\frac{(2n-1)\pi r}{2r_s}. \qquad (55)$$

This $\phi_t(r)$ does not automatically satisfy the cusp condition (29). We may therefore adopt either of two variational strategies: i) vary m chosen parameters in $\phi_t(r)$ while imposing one constraint (normalization), or ii) increase the variational sum by one term, vary m+1 parameters, and impose two constraints (normalization, and the cusp condition). In either case the variational problem is straightforward and the results are actually quite similar. This technique can easily be checked by using it to recalculate $E_0(r_s)$ for the Coulomb potential itself. With M = 5 in the sum, the variational and truncated series results differed by only parts per million throughout the range $0 < r_s < 5$. The $r_s = 1.5$ variational

wave function cannot be distinguished from figure 1 because of the width of the tracing pen.

The Hartree integral (36) and the "screening correction" integral (44) are straightforwardly computed from the $\hat{k} = \hat{0}$ variational wave function. The only remaining obstacle is the effective mass, which can again be found by integrating (32) numerically. Alternatively, the band width (and hence m^*) may be calculated from an isotropic two plane wave model appropriate for a spherical Brillouin zone.[16] If K is the magnitude of the shortest reciprocal lattice vector (so that K/2 is the radius of the first Brillouin zone and $\frac{4}{3}\pi r_s^3 \cdot \frac{4}{3} = (K/2)^3 = (2\pi)^3$), then in this model the energy $\hat{E}(k)$ relative to $\hat{V}(\hat{k} = \hat{0})$ is given by

$$\hat{E}(k) = \frac{\hat{E}_0(k) + \hat{E}_0(k-K)}{2} - \left[\left(\frac{\hat{E}_0(k) + \hat{E}_0(k-K)}{2}\right)^2 + \hat{V}^2(K)\right]^{1/2} \qquad (56)$$

where $\hat{E}_0(k) = k^2$ and $\hat{V}(k)$ is the Fourier transform of the potential. From (56) we find an approximate band width,

$$E_w = \hat{E}_0(K/2) - \left|\hat{V}(K)\right| - \hat{E}(0) = \frac{m}{m^*}(K/2)^2, \qquad (57)$$

which defines the effective mass m^*. The results of the two methods are rather similar (the two effective masses differ by 5% at $r_s = 1.5$). In the following we will use the results of the first method.

The ground state energy of this last model is again plotted in figure 3. The minimum falls at $r_s = 1.61$, where $E^0 = -1.038$ Ry, a value which is in close agreement with the results of Tua and Mahan.[4]

V. CONCLUSIONS

It is worth emphasizing that the work reported here is not a statistical mechanical calculation. We do not examine all possible states of H and find which is the most probable. Instead we have proceeded from the assumption that the most probable state for the density range of interest is a metallic one in which the protons occupy the sites of a Bravais lattice. The spherical cell approximation obviously eliminates any reference to the choice of Bravais lattice, and also eliminates the possibility that the ground state is some other configuration, such as a lattice with a diatomic basis (which is the experimental structure at zero temperature and atmospheric pressure) or a "liquid" in which the proton disorder is due not to thermal agitation, but to quantum fluctuations.[17] It is thus not surprising that our curves show physically irrelevant negative pressure for r_s greater than about 1.65. This simply reflects the well-known fact that at these densities the ground state is not a Bravais lattice metal, but is either a molecular solid or a metal in coexistence with such a solid. To complete the equation of state for hydrogen, then, we need to find $E^0(r_s)$ for a lattice with a diatomic basis,[18] and connect the two curves using a Gibbs tangent construction. Of course, there remains always a possibility that a third configuration, with still lower energy, is the true ground state. Accordingly our calculations do not profess to find the zero temperature equation of state for hydrogen, but rather the ground state energy of electrons in the presence of a putative static Bravais lattice of protons. (The major difference between this model and a plausible picture of metallic hydrogen is the lack of ionic motion.) The results do, however, show that if metallic hydrogen exists in a stable

or metastable state, then it must have a density greater than about 0.60 gm/cm^3 (which corresponds to $r_s = 1.65$).

ACKNOWLEDGMENTS

We wish to thank Dr. A.E. Carlsson for helpful conversations, Professor M. E. Fisher for encouragement, and T.G. Thomson for computer assistance. This work was supported in part by the National Science Foundation through Grant #DMR-79-24008 administered by the Materials Science Center at Cornell University, and in part by the National Aeronautics and Space Administration through Grant #NAG 2-159.

REFERENCES

1. E. Wigner and H.B. Huntington, J. Chem. Phys. 3, 764-770 (1935).
2. G.A. Neece, F.J. Rogers and W.G. Hoover, J. Comp. Phys. 7, 621-636 (1971); M. Ross and A.K. McMahan, Phys. Rev. B 13, 5154-5157 (1976); M. Ross and C. Shishkevish, Molecular and Metallic Hydrogen (Rand Corporation, Santa Monica, Calif. 1977); D.M. Straus and N.W. Ashcroft, Phys. Rev. Lett 38, 415-418 (1977); D.M. Wood, Ph.D. thesis, Cornell University, 1981 (unpublished); S. Chakravarty, J.H. Rose, D. Wood and N.W. Ashcroft, Phys. Rev. B 24, 1624-1635 (1981).
3. J. Hammerberg and N.W. Ashcroft, Phys. Rev. B 9, 409-424 (1974).
4. P.F. Tua and G.D. Mahan, Physica Status Solidi B 105, 769-775 (1981).
5. J. Bardeen, J. Chem. Phys. 6, 367-371 (1938).
6. G.D. Mahan, Many-Particle Physics (Plenum, New York, 1981), chapter 5.
7. P. Vashishta and K.S. Singwi, Phys. Rev. B 6, 875-887 (1972).
8. C.A. Sholl, Proc. Phys. Soc. 92, 434-445 (1967).
9. See also D. Pines and P. Nozières, The Theory of Quantum Liquids (Benjamin, New York, 1966), section 5.3.
10. As noted by C.J. Pethick (Phys. Rev. B 2, 1789-1801 (1970)) and discussed in detail by Hammerberg and Ashcroft,[3] if the coupling term has a fundamentally different symmetry from H_{eg}, then the consequent crossing of levels requires using a careful limit of finite temperature perturbation theory. The model used here preserves spherical symmetry so this difficulty is absent.
11. E. Wigner and F. Seitz, Phys. Rev. 43, 804-810 (1933).
12. We use the notation of M. Abramowitz and I. Stegun, Handbook of Mathematical Functions (National Bureau of Standards, Washington, D.C., 1972).

13. The normalization constant A can be determined from the result

$$\int_0^{y_s} e^{-y}M^2(a,b,y)dy = \sum_{n=0}^{\infty}\left[\sum_{m=0}^{n}\frac{(a)_m(a)_{n-m}\,(n+2)!}{(b)_m(b)_{n-m}\,n!(n-m)!}\right]\left[1-e^{-y_s}\sum_{\ell=0}^{n+2}\frac{y_s^{n+2-\ell}}{(n+2-\ell)!}\right]$$

where

$$(a)_n = a(a+1)\ldots(a+n-1) \quad n \geq 1$$
$$= 1 \quad n = 0.$$

14. A.E. Carlsson and N.W. Ashcroft, Phys. Rev. B 25, 3474-3481 (1982).

15. P.D. Ritger and N.J. Rose, Differential Equations with Applications (McGraw-Hill, New York, 1968), section 7-3.

16. N.W. Ashcroft and N.D. Mermin, Solid State Physics (Holt, Rinehart and Winston, New York, 1976), page 158.

17. S. Chakravarty and N. W. Ashcroft, Phys. Rev. B 18, 4588-4597 (1979).

18. This calculation has been attempted but it is quite difficult. See, for example, N.W. Ashcroft in A. Pekalski and J. Przystawa, eds., Modern Trends in the Theory of Condensed Matter (Springer-Verlag, Berlin, 1980) pp. 531-536.

FIG. 1. The band minimum wave function $\phi_0(r)$ at $r_s = 1.5$, as given by (27).

FIG. 2. Solid line: The ground state energy $E^0(r_s)$ calculated from a bare Coulomb potential using (38). Dashed line: a similar result assuming a spin aligned ground state, i.e., one with only one electron allowed in each spatial wave function.

FIG. 3. The ground state energy per proton $E^0(r_s)$ calculated in the Wigner-Seitz approximation with various one-body potentials. Solid line, Coulomb potential; dashed line, uniform background potential; dotted line, Thomas-Fermi potential. The cross marks the experimentally determined cell radius and ground state energy of solid molecular hydrogen at atmospheric pressure ($r_s = 3.118$, $E^0 = -1.1648$ Ry.) The inset shows the progression with r_s of the $\vec{k} = \vec{0}$ band minimum as determined by (28) for the pure Coulomb potential.

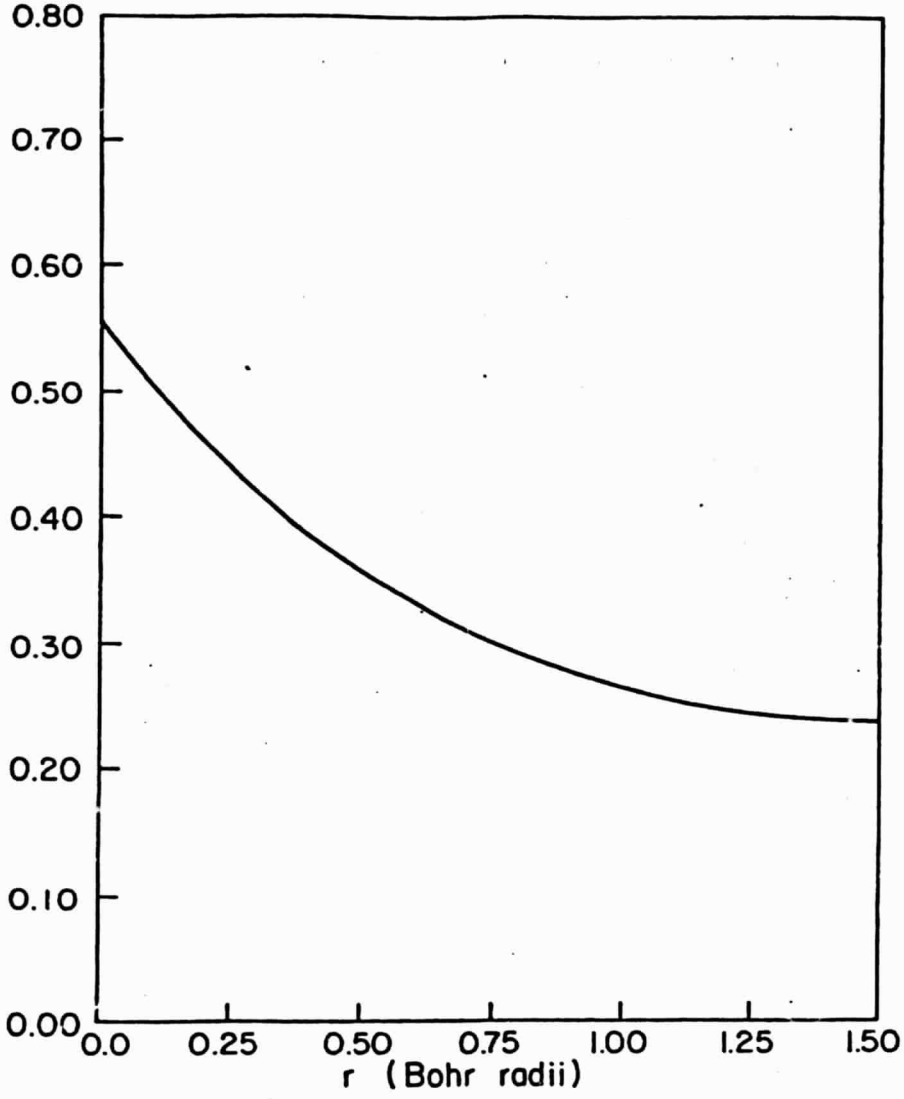

Figure 1

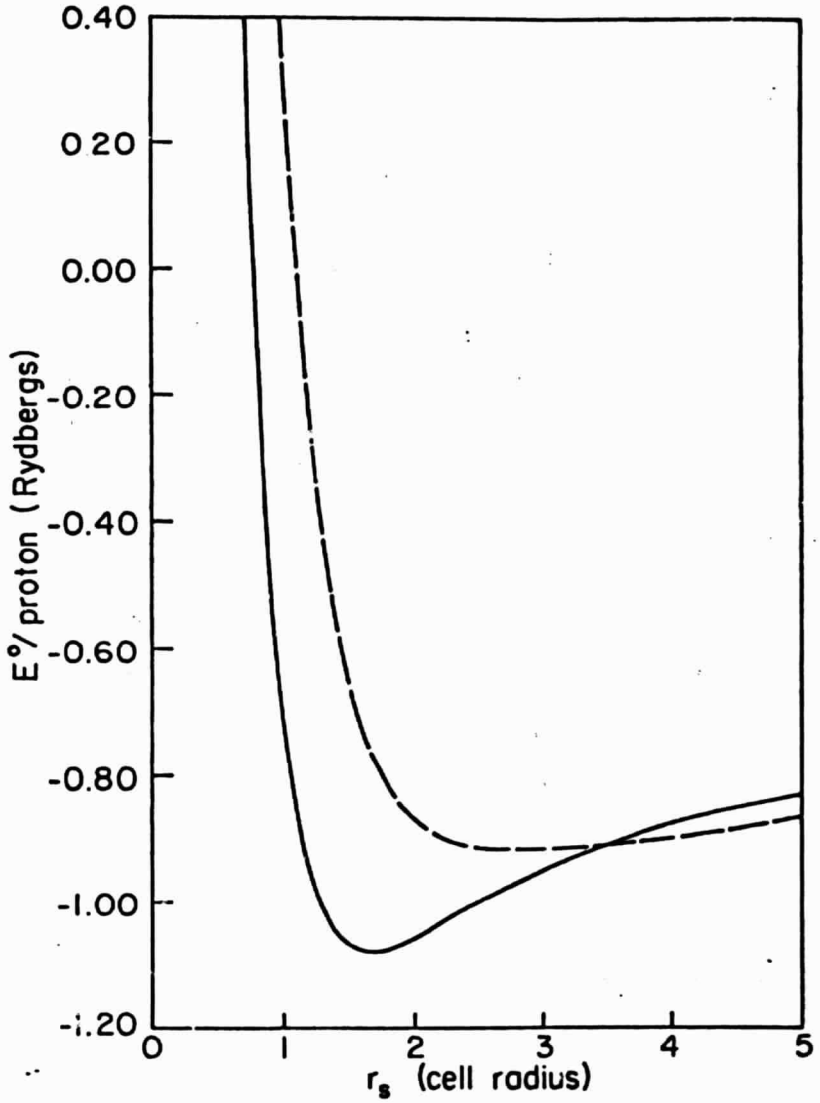

Figure 2

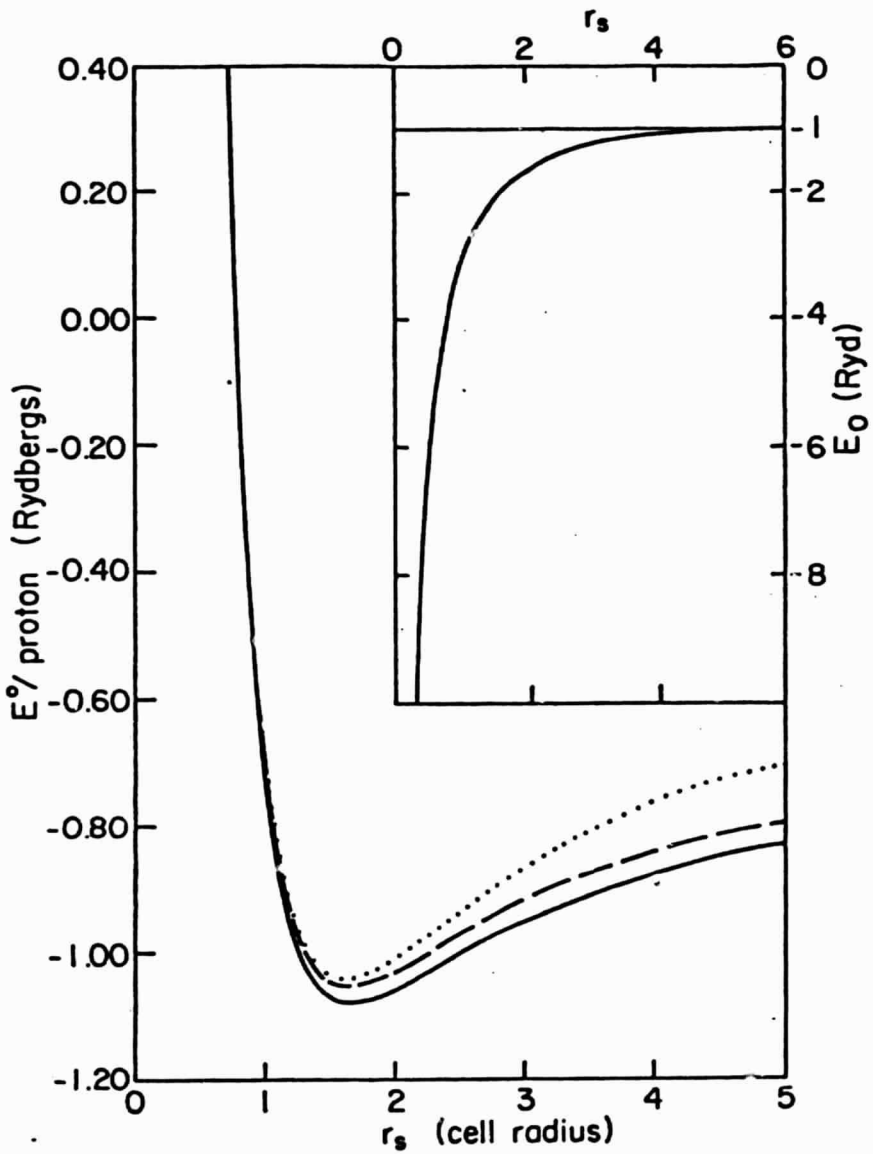

Figure 3